

MYTHO: A novel regulator of myogenesis

by

Tomer Jordi Chaffer, B.Sc. (Hons)

Centre universitaire
de santé McGill
Institut de recherche



McGill University
Health Centre
Research Institute

Division of Experimental Medicine

McGill University, Montreal

Quebec, Canada

April 2024

A thesis submitted to McGill University in partial fulfilment of the requirements of the degree of
Master of Science

© Copyright by Tomer Jordi Chaffer, B.Sc. (Hons), 2024

Table of Contents

ABSTRACT	3
RESUMÉ	5
ACKNOWLEDGEMENTS	7
CONTRIBUTION OF AUTHORS	9
LIST OF ABBREVIATIONS	12
SECTION 1: INTRODUCTION AND LITERATURE REVIEW	14
SKELETAL MUSCLE IN HEALTH AND DISEASE	14
SKELETAL MUSCLE REPAIR AND REGENERATION: THERAPEUTIC OPPORTUNITIES.....	17
ON THE ORIGINS OF <i>MYTHO</i> , A NOVEL FOXO-DEPENDENT GENE	20
AIMS OF THIS STUDY.....	23
SECTION 2: MATERIALS AND METHODS	24
CELL CULTURE.....	24
siRNA-MEDIATED RNAI.....	24
IMMUNOBLOT	25
IMMUNOFLUORESCENCE STAINING.....	27
CELL PROLIFERATION ANALYSIS.....	27
CELL CYCLE ANALYSIS	28
TRANSCRIPTOME ANALYSIS	28
IMMUNOPRECIPITATION.....	30
QUANTIFICATION AND STATISTICAL ANALYSIS	31
SECTION 3: RESULTS	32
EXPRESSION PATTERN AND LOCALIZATION OF <i>MYTHO</i> THROUGHOUT MYOGENESIS	32
VERIFICATION OF <i>MYTHO</i> KNOCKDOWN IN C2C12	32
EFFECTS OF <i>MYTHO</i> KNOCKDOWN ON THE MYOGENIC PROGRAM.....	33
EFFECTS OF <i>MYTHO</i> KNOCKDOWN ON MYOTUBE FORMATION	34
EFFECTS OF <i>MYTHO</i> KNOCKDOWN ON CELL PROLIFERATION.....	35
EFFECTS OF <i>MYTHO</i> KNOCKDOWN ON THE MYOBLAST TRANSCRIPTOME.....	35
IDENTIFICATION OF <i>MYTHO</i> INTERACTOME.....	36

SECTION 4: DISCUSSION	38
SECTION 5: REFERENCES.....	44
SECTION 6: TABLES.....	63
SECTION 7: FIGURES.....	65
SECTION 8: FIGURE LEGENDS	88

ABSTRACT

Loss of skeletal muscle mass and function is a common clinical feature and poor prognostic indicator in various pathological conditions. A promising therapeutic approach of regenerative medicine for repair of skeletal muscle is through the delivery of cellular therapies targeting regulators of muscle regeneration, a process known as myogenesis. However, not all the proteins involved in this process have been identified. Of note, the uncharacterized gene *D230025D16Rik* in *Mus musculus* or *C16orf70* in *Homo sapiens*, now termed MYTHO, has never been studied within the context of skeletal muscle growth and repair. This study provides the first assessment of the role of MYTHO in myogenesis. MYTHO expression is upregulated during differentiation and has both a nuclear and cytosolic localization during myogenesis. The role of MYTHO in a C2C12 murine model of myoblast differentiation was assessed by using a loss-of-function approach (transfection with siRNA oligos). MYTHO knockdown (MYTHO-KD) leads to early activation of the myogenic program through induction of transcription factors *MyoD1* and *MyoG* and late markers of differentiation *MyHC* and *MCK*, as determined by RT-qPCR analysis. MYTHO-KD leads to hypertrophic myotube formation as indicated by significant increases in fusion and differentiation indices and pro-differentiation genes *Mymk*, *Mymx*, *Igfbp5*, and *Fgf21*. Furthermore, MYTHO-KD reduces the proliferation capacity of myoblasts as indicated by cell number, BrdU incorporation and MTT assays, but flow cytometry shows that it does not affect cell cycle distribution. A microarray-based transcriptome profiling of MYTHO-KD myoblasts revealed marked increases in pathways related to muscle growth, differentiation, and development; and finally. Finally, proteomic screenings of MYTHO-associated proteins indicated that ATAD2, BCAS3, and the Septin family of proteins are probable interactors of MYTHO within the context of myogenesis. Altogether, these findings highlight, for the first time, the potential negative effects of MYTHO on myogenesis. The mechanistic investigations stemming from the present study will provide

further insight into the novel role played by MYTHO during skeletal muscle growth and repair. This thesis, therefore, opens up new avenues for the identification of novel therapeutic targets for prevention and potential treatment of loss of skeletal muscle mass and function.

RESUMÉ

La perte de masse et de force musculaire sont des problèmes courants qui ont un impact négatif sur la santé globale. La perte de masse musculaire peut avoir des conséquences néfastes sur la santé, notamment en augmentant le risque de chutes, de fractures, de limitations fonctionnelles et de perte d'autonomie. Il est donc important de prévenir et de traiter la perte de masse musculaire afin de maintenir une santé optimale et une qualité de vie. Une approche thérapeutique prometteuse est la médecine régénérative visant à réparer le tissu musculaire endommagé en ciblant des régulateurs de la régénération musculaire, un processus connu sous le nom de myogenèse. Cependant, toutes les protéines impliquées dans ce processus n'ont pas encore été identifiées. Il est important de noter que le gène non caractérisé D230025D16Rik chez la souris ou C16orf70 chez l'Homme, désormais appelé MYTHO, n'a jamais été étudié dans le contexte de la croissance et de la réparation musculaire squelettique. Cette étude examine le rôle de MYTHO dans la régulation de la myogenèse. En utilisant des cellules C2C12, on rapporte que l'expression de MYTHO est régulée à la hausse pendant la différenciation et que la protéine MYTHO présente une localisation nucléaire et cytosolique. L'inhibition de MYTHO (MYTHO KD) via une approche de perte de fonction (transfection avec des oligonucléotides d'ARNsi) entraîne une activation précoce du programme myogénique par l'induction des facteurs de transcription MyoD1 et MyoG ainsi que des marqueurs tardifs de différenciation MyHC et MCK. L'inhibition de MYTHO induit une hypertrophie des myotubes, telle que rapportée par l'augmentation significative de l'index de fusion et de différenciation. De plus, l'inhibition de MYTHO réduit la capacité de prolifération des myoblastes, comme montré par le nombre de cellules, l'incorporation de BrdU et les essais MTT, mais la cytométrie en flux ne montre aucune affectation au niveau de la distribution du cycle cellulaire. En utilisant une analyse transcriptomique, on rapporte que l'inhibition de MYTHO augmente plusieurs voies de

signalisation associées à la croissance, à la différenciation et au développement musculaires. De plus, nos expériences en protéomiques suggèrent que MYTHO est associées à diverses protéines, notamment ATAD2, BCAS3 et la famille de protéines Septin. Dans l'ensemble, ces découvertes mettent en évidence, pour la première fois, les effets négatifs potentiels de MYTHO sur la myogenèse. Les investigations mécanistiques issues de cette étude contribueront à une meilleure compréhension du rôle novateur de MYTHO dans la croissance et la réparation musculaire squelettique. Ces résultats ouvrent de nouvelles perspectives pour l'identification de nouvelles cibles thérapeutiques visant à prévenir et traiter la perte de masse musculaire et les dysfonctionnements musculaires squelettiques.

ACKNOWLEDGEMENTS

I would first like to express all my gratitude to my MSc supervisor, Dr. Sabah Hussain, for giving me the opportunity to be a part of his team back in 2018 when I was a young undergraduate student. A scientist, historian, and football analyst, Sabah has shared many lessons and offered mentorship and guidance whenever possible. Sabah is the best supervisor I could have ever asked for.

I am also grateful for the mentorship I have received from Dr. Jean-Philippe Leduc-Gaudet over the years. Everything I know about scientific research is from what you have taught me. You are the best teacher and mentor I could have asked for. I am looking forward to watching you become the top researcher in Canada and a global leader in the field.

The other mentor which has been vital to the production of this thesis is Dr. Alaa Moamer. Besides the technical expertise you provided for all the experiments in this thesis, you also shared many lessons about life. I am looking forward to seeing you become a top scientist and entrepreneur.

Dominique Mayaki, the engine and heart of the lab, has been kind enough to teach me all of the technical knowledge that I know today. Thank you for all the lessons, both about science and life, and for the daily conversations. Dr. Felipe Broering, the wise Brazilian master of western blot and so much more... thank you. You are a great mentor and friend for life. Dr. Sami Sedraoui, a mentor, a friend, and a football pundit, thank you for the lessons, conversations, and jokes. Thank you to Dr. Laurent Huck for the technical expertise you have provided over the years. Thank you to Sahar Mikaeeli, Aaron Wang, Marwa El Sheikh, and other students that I have collaborated with over the years. I am truly fortunate to have such great colleagues.

I address many thanks to our collaborators on the Mytho project. I am grateful to Dr. Gilles Gouspillou and all his team for the guidance throughout our weekly laboratory meetings. Many thanks to Dr. Marco Sandri, Dr. Anais Franco-Romero, and the rest of the team in Padova for the opportunity to collaborate on the Mytho project and for kindly welcoming me as a visiting student in their lab for 6 months in the beautiful country of Italy.

I address many thanks to the organizations that provided financial support for my training at McGill University, including a Graduate Fellowship from the Fonds de recherche du Québec (FRQS), a Graduate Excellence Fellowship from McGill University, and a Yvonne and Andrew Koenig Scholarship from the Jewish Community Foundation of Montreal. I also thank the organizations that provided financial support for my participation in international research activities such as conferences and my 6-month fellowship in Dr. Marco Sandri's laboratory at the Veneto Institute of Molecular Medicine of the University of Padova, including a Globalink Research Award - Marie Skłodowska-Curie Actions (MSCA) RISE from Mitacs, a Graduate Mobility Fellowship from McGill University, a Gerald B. Price Graduate Research Enhancement and Travel (GREAT) Award from the Division of Experimental Medicine, and a Till & McCulloch Meetings Trainee Award from the McGill Regenerative Medicine Network.

I am grateful to all the friends and mentors outside of the lab which have been supportive throughout the past two years. Lastly, my deepest gratitude and love to my family. To my parents, Marcelo and Claudia; my brother, Ronen; and my cat, Waska.

CONTRIBUTION OF AUTHORS

This thesis was prepared according to principles outlined in McGill University's "Guidelines for Thesis Preparation". The format conforms to "traditional monograph thesis" option. The contributions of each author are outlined below.

Tomer Jordi Chaffer (TJC): This thesis was written by M.Sc. candidate TJC, who performed literature review, prepared and revised this document. TJC optimized several laboratory experiments, performed cell culture work, siRNA transfection, qPCR, immunoblotting, and immunofluorescence, and confocal microscopy. TJC attended research team meetings, presented preliminary research findings to the M.Sc. Thesis Committee meetings and several local, national, and international conferences.

Sabah N. A. Hussain, MD, PhD (SNAH): Thesis supervisor. SNAH regularly provided mentorship, guidance and support for all experiments and sections of this thesis. SNAH also provided a supportive environment for achieving thesis objectives, attended all committee meetings, and provided extensive feedback and direction on this thesis.

Gilles Gouspillou, PhD (GG): GG provided mentorship, guidance and inputs for all sections of this thesis.

Marco Sandri, MD, PhD (MS): Research collaborator. MS provided many insightful comments and suggestions on the study design and methodology.

Alaa Moamer, PhD (AM): Post-doctoral fellow at Dr. Hussain's laboratory. Regularly provided mentorship, guidance and support for all experiments and extensive feedback on all sections of this thesis. AM provided technical expertise and assisted with cell proliferation, cell cycle, immunoprecipitation, and immunofluorescence experiments.

Jean-Philippe Leduc-Gaudet, PhD (JPLG): Former Ph.D. fellow at Dr. Hussain's laboratory and currently an Assistant Professor in the Medical Biology Department at Université du Québec à Trois-Rivières (UQTR). JPLG regularly provided mentorship, guidance and support for all experiments and extensive feedback on all sections of this thesis.

Dominique Mayaki, MSc (DM): Research assistant. DM provided technical expertise and assisted with siRNA transfection, qPCR and mRNA detection, as well provided extensive mentorship throughout MSc degree.

Laurent Huck, PhD (LH): Research associate. LH provided technical expertise and mentorship.

Felipe Broering, MD (FB): Former MSc candidate. FB provided technical expertise and mentorship.

Anais Franco-Romero (AFR): Post-doctoral fellow at Dr. Marco Sandri's laboratory. AFR provided technical expertise and mentorship.

José A. Morais, MD (JAM): Member of the M.Sc. thesis committee. JAM attended all committee meetings and provided insightful comments and suggestions on the study design.

James Martin, MD (JM): Member of the M.Sc. thesis committee. JM attended all committee meetings and provided insightful comments and suggestions on the study design.

Évelyne Vinet, MD, PhD (EV): Academic advisor member of the M.Sc. thesis committee. EV attended all committee meetings and provided insightful comments and suggestions on the study design.

LIST OF ABBREVIATIONS

AAV	Adeno-associated virus
Angpt1	Angiopoietin 1
ATAD2	ATPase family AAA domain containing 2
BCAS3	Breast carcinoma-amplified sequence 3
BSA	Bovine serum albumin
BrDu	5-Bromo-2'-Deoxyuridine (BrdU)
CDK	Cyclin-dependent kinase
C2C12	Mouse myoblasts cell line
cDNA	Complementary DNA
DAPI	4',6-diamidino-2-phenylindole
Dcn	Decorin
DNA	Deoxyribonucleic acid
ECL	Enhanced chemiluminescence
Fgf21	Fibroblast growth factor 21
FoxO	Forkhead box protein O
GAPDH	Glyceraldehyde-3-phosphate dehydrogenase
GDF11	Growth differentiation factor 11
GO	Gene ontology
H19	H19 Imprinted Maternally Expressed Transcript
IGF-1	Insulin-like growth factor 1
Igfbp5	Insulin Like Growth Factor Binding Protein 5
Igfbp2	Insulin Like Growth Factor Binding Protein 2
IPA	Ingenuity pathway analysis
KD	Knockdown
kDa	Kilo Daltons
LIR	LC3 interacting region
MCK	Muscle creatine kinase
MTT	Thiazolyl Blue Tetrazolium Bromide
mRNA	Messenger RNA
Mybph	Myosin Binding Protein H
MyHC	Myosin heavy chain
Mymk	Myomaker
Mymx	Myomixer
MyoD1	Myoblast determination protein 1
MyoG	Myogenin
MYTHO	Macroautophagy and Youth Optimizer
OD	Optical density
ORF	Open reading frame
PBS	Phosphate buffer saline
PBST	Phosphate buffer saline added Tween®20 detergent
PCA	Principal component analysis
PCR	Polymerase chain reaction
PHAF1	Phagosome assembly factor 1
PHAF2	Phagosome assembly factor 2
pRb	Retinoblastoma protein
PVDF	Polyvinylidene difluoride
RNA	Ribonucleic acid

RNAi	RNA interference
RT-PCR	Reverse transcription-PCR
Runx2	Runt-related transcription factor 2
SDH	Succinate dehydrogenase
SDS-PAGE	Sodium dodecyl sulphate polyacrylamide gel electrophoresis
SEM	Standard error of the mean
Sema3a	Semaphorin 3
Sema6a	Semaphorin 6
shRNA	short hairpin RNA
siRNA	small interference RNA
WD40	Protein domain (~40aa) terminating in WD40

SECTION 1: INTRODUCTION AND LITERATURE REVIEW

Skeletal muscle in health and disease

In the mammalian body, there are three types of muscles: skeletal, cardiac, and smooth muscles. Skeletal muscle is striated, bound to connective tissue, and composed of myofibers along with multiple different cell types that contribute to skeletal muscle homeostasis, including satellite cells, fibroblasts, lymphocytes, and many others. Skeletal muscles contain several bundles of muscle fibre rich with vascularization and innervation [1]. These bundles of muscle fibres are incredibly complex and possess many structural and functional features unique to skeletal muscle tissue.

Structurally, skeletal muscles are attached to skeletal elements, such as bones and tendons, and are broadly classified into two different fibre types. They are classified on the basis of functionality, as specified by their respective biochemical environment and physiological capacities [2]. First, there is a slow twitch (type I) skeletal muscle that function to support long distance endurance activities like marathon running. Secondly, there is fast twitch (type II) skeletal muscle that support quick, powerful movements such as sprinting or weightlifting. Furthermore, in mice, type II fibres can be classified into three major subtypes, such as types IIA, IIX, and IIB. These subtypes are classified based on expression levels of myosin heavy chain (MyHC). Another feature distinguishing fibre type is metabolic properties. For example, type I and IIA fibres are considered oxidative, whereas type IIX and IIB fibres are glycolytic. The presence of these fibres in skeletal muscle across different regions of the body is dependent on localized function, as determined by the level of exertion and type of innervation [3].

As observed in their unique structural features, skeletal muscles are incredibly dynamic and multifaceted. As such, skeletal muscles function to generate force and movement. Indeed, skeletal muscles are considered the effector organs of the locomotor system because of their

contractile properties [4]. Their contractile functions, which are rapid and voluntary, are stimulated by motor neurons upon the release the neurotransmitter acetylcholine at the neuromuscular junction [5]. In response to nerve stimulation, calcium, a signalling molecule released from the sarcoplasmic reticulum, interacts with troponin to initiate a coordinated movement with tropomyosin, whereby both elements move off the active site on the actin filament [6]. Consequently, this action allows for myosin heads to attach to active sites on actin. Thereafter, adenosine triphosphate (ATP) enables myosin to pull the actin filament toward the centre of the sarcomere. The release of an additional ATP molecule allows for the release of the myosin head and its subsequent binding to an actin site located closer to the Z-line [7]. The collective contraction of thousands of sarcomeres allows the muscle to contract through an attach-pull-release action which is repeated for multiple cycles until stimulation of the muscle stops [8]. The actomyosin contractile system is an evolved biomechanical model of motility which enables animals to interact with their environment in a dynamic nature, such as through physical movement and breathing.

In addition to their roles in facilitating movement, skeletal muscles make up a large proportion of total body mass and act as very important reserves of the energy substrates that are needed to support critical organ function. Indeed, skeletal muscles compose up to 40-50% of whole-body mass in healthy individuals [9], contain 50–75 % of all body proteins [10], and play vital roles in basic functions such as thermogenesis, endocrine signalling, and metabolism through regulation of protein, glucose, and lipid homeostasis. Given that the growth or the loss of muscle mass can influence general metabolism, locomotion, eating, and respiration [11], the maintenance of skeletal muscle mass is therefore an important determinant of quality of life.

The central mechanism regulating muscle mass and fibre size is protein turnover, the process by which the protein reservoir within skeletal muscles undergoes synthesis and degradation [12]. In most cases, muscle hypertrophy (i.e., enlargement of individual muscle

fibres) is caused by increased protein synthesis and decreased protein degradation, while muscle atrophy (i.e., decrease in muscle mass and fibre size) results from decreased protein synthesis and increased protein degradation [11].

Skeletal muscles demonstrate an incredible ability to alter their structural properties in response to the organism's homeostatic demands. Such plasticity is capacitated by the vast amounts of proteins harboured in skeletal muscles which can be modified to serve multiple functions. Skeletal muscle plasticity is exemplified by their functional capacity to adapt to stimuli in the form of load-induced stressors, substrate supplies, and environmental stressors[13]. In turn, their dynamic nature is adaptable and can take on various physiological forms, as observed in many pathological conditions where skeletal muscle structure, size, and composition are significantly altered.

Decline in skeletal muscle mass and function can lead to a poor prognosis in patients suffering from various diseases, such as cancer [14], chronic obstructive pulmonary disease [15], type 2 diabetes [16], heart failure [17], chronic kidney disease [18], immobility [19], sepsis [20], multiple sclerosis [21], neuropathies [22], osteoarthritis [23], and neuromuscular disorders [24]. Furthermore, skeletal muscle weakness, a major problem for many aged individuals, is defined as the loss of skeletal muscle function which can cause difficulties in performing normal daily functions, such as buying groceries, making the bed, or walking [25]. Such a loss of skeletal muscle mass and function is observed in sarcopenia (loss of muscle tissue as a natural part of the aging process) [26], which often leads to frailty – a risk factor for injury due to falls and immobility associated with bed rest [27].

As the maintenance of skeletal muscle health is an important determinant of quality of life [28], a decline in the maintenance of skeletal muscles can therefore lead to poor health outcomes, as observed in individuals experiencing skeletal muscle weakness [29-31]. Indeed, individuals with skeletal muscle weakness can experience a multitude of health and wellness

issues that contribute to a poorer quality of life, and, ultimately, morbidity and mortality [32-35]. Addressing the prevalence and burden on healthcare costs of muscle weakness in older adults is a growing challenge for many countries [36-39], including Canada [40]. Indeed, by 2030, it is estimated that individuals 65 years old or older will comprise almost 25% of Canada's population [41]. This is combined with the fact that up to 35% of older Canadians suffer from frailty [42]. Consequently, there is an urgent need to identify effective therapeutic strategies with immediate application for the treatment and potential prevention of loss of skeletal muscle mass and function.

Skeletal muscle repair and regeneration: Therapeutic opportunities

A promising therapeutic avenue appears to be through the delivery of cellular therapies targeting regulators of skeletal muscle regeneration. Indeed, the natural capacity of skeletal muscles to regenerate in response to injury stimuli makes them an ideal target for cell therapy [43]. Muscle regeneration involves the process of skeletal muscle stem cell (satellite cell) activation, proliferation, differentiation, and fusion into myofibers [44-46]. This process – myogenesis – is necessary for growth, repair, and maintenance of skeletal muscle mass and function throughout life (Figure 1) [47].

Upon injury, adult skeletal muscle cells do not divide as they are structurally highly differentiated; rather, these tissues hold a reservoir of quiescent satellite cells that are activated and undergo proliferation, differentiation, and fusion in order to repair injured muscle fibers (Figure 2). A common *in vivo* model for assessing the regenerative capacity of skeletal muscle is through injection of cardiotoxin (CTX), a myonecrotic agent typically extracted from *Naja mossambica mossambica* [48]. Further, intramuscular injection of glycerol has also been used as a method to induce muscle injury and regeneration [49]. In fact, satellite cells will repair and form new multinucleated myofibers within weeks [50]. First identified under electron microscopy in 1961 [51], satellite cells were named as such due to their sublamellar location

and association the plasma membrane of myofibers [52]. Since their identification, satellite cell biology has been studied quite extensively, with most efforts being placed into characterizing the dynamic interplay between satellite cells and their environment (stem cell niche). Indeed, the dynamic interplay between intrinsic signals within satellite cells and extrinsic cues originating from the stem cell niche largely regulates satellite cells during skeletal muscle regeneration [52].

Skeletal muscle injury leads external factors, such as inflammatory cells, stromal cells, trophic signals, and extracellular matrix (ECM) components to assist satellite cells through the regeneration process [53]. Intrinsically, satellite cell activation is marked by a transition from a G0 (quiescent state) to G1 (cell growth) phase of cell cycle [54]. Cell cycle re-entry is achieved through activation of cyclin dependent kinases and suppression of their inhibitors. Upon activation, satellite cells will give rise to proliferating myogenic precursor cells, known as myoblasts [55]. Proliferation is defined as the process by which a cell grows and divides to produce two daughter cells, leading to the exponential increase in the number of cells in a tissue [56]. Exposure of myoblasts to mitogenic factors, such as insulin-like growth factor, results in the dephosphorylation of FoxO1, a member of the highly conserved family of the FoxO transcription factors, which leads to reduction in the levels of cyclin-dependent inhibitors, such as p27 [57, 58]. Mitogenic factors also stimulate the progression from late G1 to S (DNA synthesis) phase of the cell cycle [59, 60]. Indeed, in response to mitogen growth factors binding to the tyrosine kinase receptor, retinoblastoma protein (pRb) is able to control the restriction point in the late stage G1-phase [61]. The phosphorylation of pRb is controlled by cyclin D-associated cyclin-dependent kinases (cdks) and cdk inhibitors, such as p21 and p16 [62, 63]. Progression into G2 (cell growth) phase is further orchestrated by growth factor-mediated and MyoD1-dependent activation of myogenic pathways and coincides with myoblast formation and proliferation. Here, cell cycle inhibitors such as p21 and p27 are

downregulated, which allows myoblasts to remain in a proliferative state, rather than transitioning to another phase of the cell cycle or exiting the cell cycle altogether [64].

Growth factor deprivation causes proliferating myoblasts to irreversibly withdraw from cell cycle and acquire an apoptosis-resistant phenotype [65]. This process is regulated by cyclin-dependent kinase inhibitors, such as p21, p19, and p57, which instruct myoblasts to undergo differentiation by facilitating cell cycle withdrawal [66-68]. Thereafter, myoblasts will begin to differentiate to form mature myocytes [69, 70]. Differentiation is broadly defined as the process by which a stem cell changes from one type to a differentiated one, typically a cellular state that is more specialized and tissue-specific [71]. This step of the myogenic lineage progression is characterized by the expression of *MyoD1* and *Myf5* transcription factors, which facilitates the transition from the quiescent, undifferentiated progenitor cells to the mature myocytes. Precisely, *MyoD1* regulates the expression of *Cdc6*, a gene involved in making chromatin accessible for DNA replication, thereby allowing cell cycle entry [54, 72]. By establishing an open chromatin structure, *MyoD1* functions to inhibit stem-cell self-renewal by signaling for expression of genes involved in myogenesis [73].

As myocytes fuse into myotubes, they continue to develop and mature by becoming multinucleated structures. Here, Myogenin orchestrates late differentiation by encoding for muscle-specific transcription factors [74, 75]. Additionally, Myomaker (*Mymk*) and Myomixer-Myomerger-Minion (*Mymx*), two well-known muscle-specific fusogenic proteins specifically expressed during myocyte fusion, follow a similar expression pattern as Myogenin [76-81]. Moreover, the fusion of myocytes and formation of myotubes during late differentiation requires permanent inhibition of cell cycle re-entry. In this step, pRb expression plays a critical role for the inhibition of DNA synthesis and commitment to the myogenic cell lineage, which coincides with induction of late differentiation markers such as myosin heavy chain (*MyHC*), a motor protein, and muscle creatine kinase (*MCK*), an enzyme [82] (Figure 2).

The skeletal muscle community has reached a consensus about the fact that the discovery and characterization of the myogenic factors involved in regulating myogenesis was enabled by the creation of the C2C12 murine myoblast cell line [83]. The original C2C12 cell line was derived from primary myoblast cultures of 2-month-old mice in 1977 by Yaffe and Saxel at The Weizmann Institute of Science in Israel [84, 85]. Since then, the C2C12 myoblast cell line has served as a valuable *in vitro* model for identifying and characterizing the underlying mechanisms of myoblast proliferation, differentiation, and fusion into myotubes [86]. The C2C12 cell line demonstrates rapid differentiation when exposed to low serum conditions [87], whereas, when exposed to high serum conditions, it demonstrates rapid proliferation [88]. Therefore, the phenotypic stability of the C2C12 cell line makes it an ideal model for studying novel genes involved in the regulation of myogenesis.

To study novel genes involved in the regulation of myogenesis, researchers have developed robust protocols involving a variety of genetic manipulation techniques known as “loss-of-function” experimental models. In these models, genetic manipulation techniques can be used to silence the expression of target genes, which is known as knocking down [89]. This can be achieved by using RNA interference (RNAi), a process where mRNA encoded by the target gene is degraded by double-stranded RNA (dsRNA) [89]. As such, characterizing the role of novel genes involved in myogenesis using a loss-of-function approach in C2C12 myoblasts is a valuable tool for identifying novel therapeutic targets involved in skeletal muscle growth and repair.

On the origins of *Mytho*, a novel FoxO-dependent gene

The characterization of myogenesis-related genes, and their functions, is essential for the understanding of molecular mechanisms that regulate satellite cell activation, proliferation, differentiation, and fusion into myofibers. One gene that demonstrates potential to play a role in myogenesis was recently identified in transcriptomic screenings performed by Dr. Marco

Sandri's research group, which revealed a novel gene that was downregulated in a triple Forkhead Box O transcription factors 1, 3 and 4 muscle-specific knockout (FoxO1,3,4^{-/-}) mice under acute starvation conditions [90]. Preliminary and currently unpublished experiments from Sandri's research group showed that this gene plays important roles in autophagy (recycling of dysfunctional proteins and organelles) and longevity. Hence, this gene, *D230025D16Rik* or *C16orf70*, has been termed MYTHO, which stands for **M**acroautophagy and **Y**ou**TH** **O**ptimizer.

MYTHO is highly conserved in various species; for example, both the nematode, *Caenorhabditis elegans* and the flowering plant, *Arabidopsis thaliana* have ~95% amino acids sequence similarity with humans. The human ortholog of MYTHO is *C16orf70* (chromosome 16 open reading frame 70) and it belongs to UPF0183 family of proteins. MYTHO has a length of 422 amino acids and a molecular weight of 47.5 kilo dalton (kDa). Our bioinformatic assessment of MYTHO using *Ensembl* (<https://ensembl.org/>) revealed two functional murine isoforms, D230025D16-201 and D230025D16-203 (Figure 4), with MYTHO isoform D230025D16-201 being more abundant than D230025D16-203 at the mRNA level in C2C12 (Figure 5). Furthermore, MYTHO contains several WD40 repeats (also known as WD or beta-transducin repeats) and putative light chain 3 (LC3)-interacting region (LIR) motifs (Figure 3B). WD40 domains provide various protein-protein or protein-DNA interaction platforms [91], which, in turn, enable proteins to have diverse functions, such as in signal transduction or in transcriptional regulation of genes involved in apoptosis, autophagy, and the cell cycle [92]. Moreover, LIR motifs are essential for protein interactions pertaining to autophagy [93].

In a study published in the journal *Autophagy*, Yamada and Schaap (2020) studied a genetic lesion in a deeply conserved gene of unknown function, named *KinkyA* (*KnkA*), which is the *Dictyostelium* ortholog of *D230025D16Rik*. In their study, the authors provided experimental evidence for the essential role *KnkA* plays in spore autophagy and differentiation

by utilizing a loss-of-function approach [94]. The authors also experimentally confirmed, for the first time, that *KnkA* interacts with BCAS3 (microtubule associated cell migration factor), a protein interaction detected previously in various proteomic screenings [95-97]. A subsequent study published in *Autophagy* by Kojima *et al.* (2021) reported that C16orf70 and BCAS3 form a complex that associates with the phagophore assembly site during autophagy [98]. Due to their reported findings, C16orf70 and BCAS3 have been termed **PHagosome Assembly Factors 1 and 2** (PHAF1/PHAF2), respectively. In a reciprocal human open reading frame (ORF)ome v1.1 screening, MYTHO was found to have potential interactions with ataxin-3, a protein implicated in the pathophysiology of cerebellar Purkinje cell (PC) degeneration [99]. Further investigations revealed that MYTHO may be implicated in the pathophysiology of spinocerebellar ataxias (SCAs), a group of inherited neurodegenerative diseases, by influencing the cytotoxicity of pathogenic ataxin-1 [100]. Recent protein-protein detection screenings relevant to neurodegeneration also detected an interaction between MYTHO and ataxin-3 [101]. Furthermore, whole genome methylation analyses of schizophrenia patients with complete remission and control male pool before treatment determined that *C16orf70* is a differentially methylated region (DMR) [102].

Recently, our group (Leduc-Gaudet, Franco-Romero, *et al.* (2023)) is the first to explore the functional importance of MYTHO in skeletal muscles *in vivo*. Indeed, Leduc-Gaudet and colleagues established the short term and prolonged depletion models by knocking down MYTHO (MYTHO-KD) expression using AAV-mediated transduction of MYTHO small hairpin RNAs (sh-RNA) oligos in mouse skeletal muscle for various durations of 3-, 6-, 12-, and 20 weeks. Interestingly, short-term depletion of MYTHO in mice attenuated muscle atrophy caused by fasting, denervation, cancer cachexia and sepsis, while prolonged MYTHO depletion resulted in excessive muscle growth, impaired muscle contractility, and several severe myopathic features, such as inflammation, degeneration/regeneration, and tubular

aggregates [103]. Based on these observations, the authors established that MYTHO is a key player in the maintenance of skeletal muscle homeostasis, mainly by regulating autophagy, skeletal muscle mass, and integrity.

To address the mechanisms underlying muscle hypertrophy and myopathic features induced by MYTHO-KD, Leduc-Gaudet and colleagues performed microarray analyses on GAS muscle samples obtained three- and twelve weeks post MYTHO-KD. Interestingly, prolonged MYTHO-KD altered the expression of several genes involved in skeletal muscle growth and development, such as ones associated with tissue regeneration and cell differentiation pathways. In light of this observation, our research team questioned whether MYTHO plays a role in regulating formation, growth, and development of skeletal muscle tissue (i.e., myogenesis).

Aims of this study

To further explore the link between MYTHO and myogenesis, we set out to characterize the involvement of MYTHO in a C2C12 model of myoblast differentiation. To assess the functional role of MYTHO during myogenesis, we utilized an siRNA loss-of-function approach to decrease the expression of MYTHO during a 7-day time-course of C2C12 myoblast differentiation. Moreover, will used a variety of experimental methods to assess the uncharacterized role of MYTHO during myogenesis.

SECTION 2: MATERIALS AND METHODS

Cell Culture

The C2C12 cell line (CRL-1772™, ATCC, Manassas, VA, USA) was sustained by passaging and culturing on a standard 50mm non-treated petri dish (101IRR, Thermo Fisher Scientific, Saint-Laurent, QC, Canada) in growth media consisting of Dulbecco's Modified Eagle's Medium (DMEM) (Gibco, 41966029, Thermo Fisher Scientific, Saint-Laurent, QC, Canada) containing 10% fetal bovine serum (Life Technologies, 16010-159) and antibiotic/antimycotic (Life Technologies, 15240-062). Passaging is initiated by the splitting of a maximum of 70% confluent cells. The cells were incubated at 37 °C with 7.5% CO₂ until they reached the desired confluence for transfection (80-90%). All experiments were conducted on C2C12 under passage 10. To induce differentiation, the cells must reach 100% confluence before switching to differentiation medium consisting of DMEM, 2% Horse Serum (16050130, Thermo Fisher Scientific, Saint-Laurent, QC, Canada), and antibiotic/antimycotic. The cells were replenished with fresh differentiation medium daily for 7 days.

siRNA-mediated RNAi

C2C12 cells were seeded in either 12-well plates (150628, Thermo Fisher Scientific, Saint-Laurent, QC, Canada) for PCR analysis, 6-well plates (140675, Thermo Fisher Scientific, Saint-Laurent, QC, Canada) for immunoblot analysis, or 35 mm petri dish, 14 mm Microwell (MaTek Corporation, Ashland, MA, USA) plates for immunofluorescence staining. The number of cells plated was 15×10^4 and myoblasts were transfected with Lipofectamine™ RNAiMAX Transfection Reagent (13778075, Thermo Fisher Scientific, Saint-Laurent, QC, Canada) at around 90% confluence. The concentration for both control (AM4611, Ambion, Thermo Fisher Scientific, Saint-Laurent, QC, Canada) and MYTHO (4390771, Ambion, Thermo Fisher Scientific, Saint-Laurent, QC, Canada) siRNAs was 20nM. For 12-well plates,

275 μL of DMEM (without serum) was added to each well. In one Eppendorf tube, 10 μL of *Mytho* siRNA and 1500 μL of GIBCO Opti MEM (31985062, ThermoFisher Scientific, Saint-Laurent, QC, Canada) were mixed for 5 min. In another Eppendorf tube, 40 μL of RNAiMAX and 1500 μL of GIBCO Opti MEM were mixed for 5 min. Subsequently, both solutions were transferred into one Eppendorf tube and mixed thoroughly. After 20 min, 125 μL of the solution was added into each well. The same procedure was followed for negative control (scramble siRNA) condition. The cells were incubated for a minimum of 12 hours before addition of 500 μL of Full DMEM. Forty-eight hours after transfection, cells were switched to differentiation medium.

Immunoblot

C2C12 myoblasts were harvested by aspirating medium and adding 200 μL of fresh BLB lysis buffer (50 mM Hepes, 150 mM NaCl, 100mM NaF, 5 mM EDTA, 0.5% Triton X-100, 0.1 mM DTT, 2 $\mu\text{g}/\text{mL}$ leupeptin, 100 $\mu\text{g}/\text{mL}$ PMSF, 2 $\mu\text{g}/\text{mL}$ aprotinin, and 1 mg/100 mL pepstatin A, pH 7.2). The 6-well plates were then placed on a shaker until the mixture of cells and BLB lysis buffer reached a viscous consistency. Each mixture was transferred to a corresponding Eppendorf tube. Mixtures were centrifuged at 5000 G for 5 min at 4 $^{\circ}\text{C}$ to remove debris from lysate mixture. The supernatants were collected, and the pellets were discarded. To determine the total protein concentration of each sample, a Bradford assay technique was performed using Coomassie Blue G-250 reagents (Bio-Rad, Hercules, California, United States) according to manufacturer's instructions. Concentrations were measured on a Tecan Infinite M200 Plate Reader using 595 nm absorption setting (Tecan, Männedorf, Switzerland). A 1 $\mu\text{g}/\mu\text{L}$ mix was prepared using crude homogenate samples, 6X SDS sample buffer (J61337.AC, Thermo Fisher Scientific, Saint-Laurent, QC, Canada), and H_2O . The samples were boiled for 7 min at 95 $^{\circ}\text{C}$.

Equal amounts of denatured protein extracts (30 µg per lane) and 7 µL of molecular weight ladder (Bio-Rad, Hercules, California, United States) were loaded on 10-well tris-glycine sodium dodecyl sulfate polyacrylamide (SDS-PAGE) 8–16% Mini-PROTEAN® TGX™ Precast Protein gels (4561104, Bio-Rad, Hercules, California, United States) and separated by electrophoresis (164-5050 PowerPac™ Basic Power Supply, Bio-Rad, Hercules, CA) at 70V and 300mA for 2 hours. A wet transfer technique was employed using polyvinylidene difluoride (PVDF) membranes (Bio-Rad Laboratories, Saint-Laurent, QC, Canada) in the presence of a power supply (PowerPac™ Basic Power Supply, Bio-Rad, Hercules, CA) at 70V and 300mA for 2 hours at 4 °C.

After the transfer, a Ponceau-S stain technique was conducted to detect the total protein on the membrane. The membrane was placed in the Ponceau S staining solution (#P3504, MilliporeSigma, Darmstadt, Germany) for 5 min on a shaker, followed by a light wash with H₂O to remove excess Ponceau S reagent. The membrane was imaged on a ChemiDoc™ XRS+ Imaging System (Bio-Rad, Hercules, California, United States). The membranes were blocked in Phosphate-buffered saline (PBS) + 1% Tween® 20 (P9416-50ML, MilliporeSigma, Darmstadt, Germany) + 5% bovine serum albumin (BSA) (23210, Thermo Fisher Scientific, Saint-Laurent, QC, Canada) on the shaker for 45 min at room temperature, followed by incubation with specific primary antibodies overnight at 4 °C on the shaker (See Appendix). On the next day, the membranes were washed in 10% PBST (3 × 5 min), followed by a 45 min incubation at room temperature with horseradish peroxidase (HRP)-conjugated secondary anti-rabbit antibody (See Appendix). The membranes were washed in 10% PBST (3 × 5 min) before imaging. The membranes were placed in Pierce™ ECL Western Blotting Substrate (32209, Thermo Fisher Scientific, Saint-Laurent, QC, Canada) for 5 min before immunoreactivity detection on a ChemiDoc™ XRS+ Imaging System (Bio-Rad, Hercules, California, United States) using the auto exposure setting.

Immunofluorescence Staining

Transfected C2C12 myoblasts cultured in 35 mm petri dish, 14 mm Microwell were washed with 1X PBS (10010072, Thermo Fisher Scientific, Saint-Laurent, QC, Canada) at approximately 1 mL for each well. The cells were fixed in room temperature 4% paraformaldehyde/PBS (30525-89-4, MilliporeSigma, Darmstadt, Germany) at approximately 1 mL for each well at room temperature for 10 min. Then, cells were washed with room temperature 1X PBS for 5 min \times 2. After this step, the fixed cells were kept in 1X PBS at 4 °C if the staining was to be performed at a later date. To proceed with the staining, the cells were permeabilized in 0.2% Triton/PBS (28314, Thermo Fisher Scientific, Saint-Laurent, QC, Canada) for 5 min. The cells were then washed with 1X PBS quickly prior to blocking.

To block for non-specific binding, the cells were incubated in 5% Normal Donkey Serum (NDS)/PBS (approximately 150 μ L per well) for 1 hour. Then, primary MF20 antibody (2 μ g/mL) in 5% NDS/PBS was applied at 150 μ L per well for 1 hour at room temperature (See Appendix). The plates were covered in tin foil to minimize exposure to light. After 1 hour, the cells were washed with PBS for 5 min \times 3. The secondary antibody, goat anti-mouse-IgG-FITC (See Appendix) and DAPI (4',6-diamidino-2-phenylindole) (D1306, Thermo Fisher Scientific, Saint-Laurent, QC, Canada) were diluted 1:300 in 5% NGS/PBS. The cells were incubated at room temperature for 1 hour. The cells were subsequently washed with 1X PBS for 10 min \times 3 before imaging. Images were taken using a Zeiss LSM 700 laser scanning confocal microscope and processed on ZEN lite Digital Imaging Software (Carl Zeiss, Oberkochen, Germany).

Cell Proliferation Analysis

Forty-eight hours after transfection with MYTHO siRNA and control siRNA, cell proliferation was measured by 5-Bromo-2'-Deoxyuridine (BrdU) and Thiazolyl Blue Tetrazolium Bromide (MTT) assays. For the BrdU incorporation assay, cells were trypsinized,

re-suspended and counted. 2 densities of cells were plated in 96-well plates with full growth media (2×10^5 cells/mL and 4×10^4 cells/mL in 100ul/well). Two types of controls were used to ensure the validity and specificity of the experiments: (i) control, where cells were added but not incorporated with BrdU reagent and (ii) blank, where only culture media was added. Cells were incorporated with 20 μ L of 1X BrdU reagent for 24 h before they were fixed and proceeded with detection protocol that was provided with BrdU ELISA Kit (ab126556, Abcam, UK). Each technical replicate was verified 3 times spontaneously.

For the MTT assay (V13154, ThermoFisher Scientific, Saint-Laurent, QC, Canada), MYTHO siRNA and control siRNA were plated for assay at 24, 48-, 72-, 96-, and 120-hours post plating. A concentration of 10 μ M UO126 was applied 24 hours post plating. The growth medium was removed at each timepoint and replaced with 0.5 mg/mL MTT in DMEM medium (without phenol red) for 3.5 hours. After removing the MTT solution, myoblasts were lysed with 4 mM HCl and 0.1% NP-40 in isopropanol and optical density was measured using a Tecan Infinite M200 Plate Reader at 590 nm absorption setting.

Cell Cycle Analysis

Forty-eight hours after transfection with MYTHO siRNA and control siRNA, cells were washed once with 1x PBS and fixed in 70% ethanol at 4°C overnight. The following day, cells were resuspended with 1x PBS and incubated with propidium iodide (PI) in the presence of RNase A at 37°C for 30 minutes, and then DNA content was analyzed using the FACS Aria Fusion flow cytometer (Becton Dickinson, NJ) with the FACSDiva software at the RI-MUHC Centre for Translational Biology Technology Platforms.

Transcriptome Analysis

Forty-eight hours after transfection, samples were harvested for microarray Affymetrix Mouse Clariom S Array (Affymetrix Onc., Santa Carla, CA, USA). RNA preparation and

hybridization were performed according to the manufacturer's protocol. All microarray analyses were performed by the Canadian Centre for Computational Genomics (C3G; Genome Quebec). Pre-processing of raw gene expression data of 22,206 mouse genes was conducted in the Transcriptome Analysis Console (TAC) 4.0.1. To identify differential expression between scramble and MYTHO KD C2C12 myoblasts, the R package limma was used [104]. Benjamin-Hochberg method was used to correct nominal p-values for multiple testing. Genes showing an FDR < 0.05 were considered significantly differentially expressed.

All the significantly differentially expressed genes from the microarray were inputted into Metascape online software to identify pathways and biological processes that were significantly altered [105]. Metascape first converted inputted identifiers into Human Entrez Gene ID. Input identifiers were mapped into human based orthologs on the latest NCBI Homologene. All statistically enriched Gene Ontology terms, accumulative hypergeometric p-values, and enrichment factors were calculated and used for filtering. The remaining significant terms were then hierarchically clustered into a tree based on Kappa-statistical similarities among their gene memberships.

For each given gene list, pathway and process enrichment analysis was carried out with the following ontology sources: Kyoto Encyclopedia of Genes and Genomes (KEGG) Pathway (<https://www.genome.jp/kegg/>), Gene Ontology (GO) Biological Processes (<http://geneontology.org/>), Reactome Gene Sets (<https://reactome.org/>), Comprehensive Resource of Mammalian Protein Complexes (CORUM) (<https://mips.helmholtz-muenchen.de/corum/>), and Transcriptional Regulatory Relationships Unraveled by Sentence-based Text Mining (TRRUST) (<https://www.grnpedia.org/trrust/ontology>). Terms with a p-value < 0.01, a minimum count of 3, and an enrichment factor > 1.5 (the enrichment factor is the ratio between the observed counts and the counts expected by chance) are grouped into clusters based on their membership similarities. P-values are calculated based on the

accumulative hypergeometric distribution, and q-values are calculated using the Benjamini-Hochberg procedure to account for multiple testing. Kappa scores are used as the similarity metric when performing hierarchical clustering on the enriched terms, and sub-trees with a similarity of > 0.3 are considered a cluster. The most statistically significant term within a cluster is chosen to represent the cluster. All heat maps were generated using the following website: <https://software.broadinstitute.org/morpheus/>. The Ingenuity Pathway Analysis (IPA) was performed using IPA Analysis MatchExplorer NUL for Network Analysis according to software instructions (830018, Qiagen, Germantown, MD, USA).

Immunoprecipitation

C2C12 were seeded in 50mm petri dishes until reaching 80-90% confluence. Three samples were harvested: at the myoblast phase, 12 hours after addition of differentiation medium, and at 5 days after addition of differentiation medium. Cells were washed once with PBS before addition of fresh RIPA buffer (sodium chloride (5 M), Tris-HCl (1 M, pH 8.0), nonidet P-40, 10% sodium deoxycholate, 10% SDS) with protease and phosphatase inhibitors (#5872, Cell Signaling, MA). Samples were centrifuged at 7000 RPM for 25 min and supernatant was transferred to a new Eppendorf tube. A volume of 30 μ L of pre-washed Dynabeads™ (10001D, ThermoFisher Scientific, Saint-Laurent, QC, Canada) was added to the samples and then placed on a rotator at 4°C for 1 hour. Subsequently, samples were centrifuged at 15000 RPM for 1 min, and the supernatant was transferred to a new Eppendorf tube. Samples were incubated with either Recombinant Anti-C16orf70 (ab181987, Abcam, UK) or isotype control Normal Rabbit IgG antibody (#2729, Cell Signaling, MA) overnight at 4°C. The antibodies were added at a concentration of 10 μ L per 1 mL of sample lysate. The following day, samples were washed with HNTG buffer (50 mM HEPES (pH 7.5), 150 mM NaCl, 0.1% Triton X-100 and 10% (vol/vol) Glycerol) with protease and phosphatase inhibitors (#5872, Cell Signaling, MA), including a series of centrifugations at 15000 RPM for

30 seconds. Samples were analyzed using the EVOQ Triple Quadrupole mass spectrometer (Bruker Daltonics, MA, USA) at the RI-MUHC Centre for Translational Biology Technology Platforms. Proteomics data was visualized using Scaffold Viewer 5.3.0 software.

Quantification and statistical Analysis

The optical densities (OD) of the protein bands were quantified using ImageLab software (Bio-Rad Laboratories) and normalized to loading controls (GAPDH or B-Tubulin). Immunoblotting data are expressed as relative to control siRNA. The quantification of Myogenin positive cells was calculated as the percentage of the number of Myogenin expressing myoblasts over the total number of myoblasts. The fusion index was manually calculated as the percentage of the number of myosin heavy chain expressing myotubes with greater than 2 nuclei divided by the total number of nuclei. The differentiation index was manually calculated as the percentage of the number of nuclei in myotubes expressing myosin heavy chain divided by the total number of nuclei in a field.

All statistical analyses were performed using GraphPad Prism (Prism 8, GraphPad Software, CA, USA). An unpaired T test was performed to compare the effect of MYTHO siRNA and control siRNA on the expression of MYTHO and myogenesis-related genes. This test was followed up with a post-hoc analysis correction by a two-stage linear step-up procedure of Benjamini, Krieger, and Yekutieli method to correct false discovery rate (Desired FDR (Q) 1.00%) with correction for multiple samples.

SECTION 3: RESULTS

Expression pattern and localization of MYTHO throughout myogenesis

To study the functional importance of MYTHO throughout myogenesis, we set out to characterize the mRNA and protein expression patterns and localization of MYTHO throughout differentiation. As depicted in Figure 7 A&B, MYTHO expression is elevated when differentiation is induced through deprivation of growth factors. Furthermore, MYTHO mRNA levels are also induced in response to differentiation, while remaining constant across the differentiation time course (Figure 8).

To determine the localization of MYTHO throughout myogenesis, we performed immunofluorescence staining for MYTHO in myoblasts and myotubes. In myoblasts, MYTHO protein displayed a nuclear localization, while in myotubes, MYTHO protein appeared to have a positive signal in both the nucleus and cytoplasm (Figure 9).

Verification of MYTHO knockdown in C2C12

To study the functional importance of MYTHO during differentiation, we transfected C2C12 myoblasts with siRNA oligos targeting D230025D16Rik to knockdown (KD) MYTHO expression over a 7-day time course of differentiation. The siRNA oligos targeting D230025D16Rik are selective for the *Mytho* murine isoform D230025D16-201, as shown in Figure 6 showing mRNA levels of *Mytho* murine isoforms D230025D16-201 and D230025D16-203 in C2C12 myoblasts transfected with MYTHO siRNA oligos. To confirm transfection efficiency over a 7-day time course of differentiation, we first evaluated the mRNA level of MYTHO in response to transfection with *Mytho* siRNA and control siRNA at day 0, 1, 3, 5, and 7 of differentiation. *Mytho* mRNA levels were significantly downregulated in response to transfection with siRNA-*Mytho* oligos, as compared to transfection with scramble siRNA oligos, at each time point over a 7-day time course of differentiation (Figure 10C) ($P <$

0.05). To evaluate the transfection efficiency at the protein level, we evaluated the expression of MYTHO by immunoblot (Figure 10A). Figure 10B shows that we achieved a 50% reduction in the level of MYTHO protein content at day 0 ($P < 0.05$). To further confirm our knockdown approach, we visualized MYTHO protein in control and MYTHO-KD myoblasts by immunofluorescence. Figure 10D depicts representative images of MYTHO in the nuclei of control myoblasts, whereas MYTHO-KD myoblasts exhibit a reduction in positive MYTHO signal.

Effects of MYTHO knockdown on the myogenic program

To investigate the effect of MYTHO knockdown on the myogenic program, we detected the expression of four myogenic genes: myoblast determination protein 1 (*MyoD1*), Myogenin (*MyoG*), myosin heavy chain 1 (*MyHCI*), and muscle creatine kinase (*MCK*) in response to transfection with siRNA-Mytho oligos at each time point over a 7-day time course of differentiation. All four myogenic genes were significantly upregulated in response to MYTHO knockdown at day 0 (Figure 11). The effect of MYTHO knockdown on all four myogenic genes became less pronounced over the time course of differentiation (i.e., day 1, 3, 5, and 7).

As compared to transcription factor MyoD1, which had less than a 1-fold increase on day 0, transcription factor Myogenin exhibited nearly a 10-fold increase day 0. To evaluate whether the increase in Myogenin was consistent at the protein level, we performed immunostaining for Myogenin at day 0. Figure 12 A&B show that transfection with siRNA-Mytho oligos led to a significant increase in the number of Myogenin positive myoblasts (i.e., myoblasts expressing Myogenin) at day 0, indicating an early activation of the myogenic program.

Effects of MYTHO knockdown on myotube formation

To visualize the phenotype of MYTHO-KD cells that display an early commitment to the myogenic program, we employed an immunofluorescence staining for MyHC1, a marker of late differentiation, in response to transfection with siRNA-Mytho oligos at day 0 and day 1 of differentiation. Confocal microscopy images revealed that myotubes formed at day 0 in response to transfection with siRNA-Mytho. On day 1, large, multinucleated myotubes formed in response to the transfection with siRNA-Mytho, while myoblasts transfected with siRNA-Control did not appear to form any myotubes, as indicated by the lack of MyHC1 signal (Figure 13).

We quantified the effect of MYTHO-KD on the rate of myotube fusion by calculating the fusion index (i.e., the number of myosin heavy chain expressing myotubes with greater than 2 nuclei divided by the total number of nuclei) in response to transfection with siRNA-Mytho oligos at day 0 and day 1 of differentiation. As shown in Figure 14A, the fusion index was significantly increased on day 0 and day 1. To quantify the effect of MYTHO-KD on the differentiation of myoblasts into myotubes, we calculated the differentiation index (i.e., the number of nuclei in myotubes expressing myosin heavy chain divided by the total number of nuclei in a field) in response to transfection with siRNA-Mytho oligos at day 0 and day 1 of differentiation. Like the fusion index, we also detected an increase in the differentiation index at day 0 and 1, as shown in Figure 14B.

To assess potential mechanistic targets mediating the effect of MYTHO-KD on the formation of large, multinucleated myotubes at early time points of myogenesis (i.e., day 0 and day 1), we detected the expression of genes known to promote myotube growth and formation: Myomaker (*Mymk*), Myomixer (*Mymx*), Fibroblast growth factor 21 (*Fgf21*), and insulin like growth factor binding protein 5 (*Igfbp5*). As depicted in Figure 15, all four myogenic genes were significantly upregulated in response to MYTHO-KD at day 0.

Effects of MYTHO knockdown on cell proliferation

To evaluate the effects of MYTHO-KD on the proliferative phase of myogenesis, we employed cell counting and BrdU incorporation assay. Cell counting revealed a significant decrease in MYTHO-KD as compared to control myoblasts (Figure 16A). Supporting this finding, a quantitative analysis of C2C12 myoblast proliferation using the MTT assay revealed a decrease in the proliferation capacity of MYTHO-KD myoblasts (Figure 16B). BrdU incorporation assay also revealed a reduction in the proliferative capacity of MYTHO-KD myoblasts (Figure 16C).

To assess whether the reduction in cell proliferation observed in MYTHO-KD myoblasts was caused by an early withdrawal from the cell cycle, we performed an analysis of cell cycle through RT-qPCR of various cell cycle genes and flow cytometric quantitation of DNA content by DNA-binding fluorochrome, propidium iodide (PI). While an RT-qPCR screening of cell cycle genes revealed a significant reduction in the mRNA level of CyclinD1 (*CCND1*) (Figure 16D), a flow cytometric quantitation of DNA content by PI did not reveal any significant differences between MYTHO-KD and control myoblasts with respect to the G₁, S and G₂ stages of cell cycle (Figure 16E).

Effects of MYTHO knockdown on the myoblast transcriptome

To evaluate the effects of MYTHO-KD on the myoblast transcriptome, we employed a microarray-based transcriptome analysis at 48-hours post-transfection with siRNA-*Mytho* oligos. A Principal Component Analysis (PCA) of the output from our Affymetrix Mouse Clariom S Array of *Mytho* siRNA and control siRNA samples was carried out to reduce the dimensionality of our dataset while preserving maximum variation (Figure 17A). Figure 17B demonstrates the efficiency of our siRNA-based transfection approach as *Mytho* is the second most downregulated gene detected in our microarray. The heatmap in Figure 18 further

supports this, while also showing the top 50 significantly differentially expressed genes in response to transfection with siRNA-Mytho oligos.

Among the top 50 significantly expressed genes, various promoters of differentiation and negative regulators of proliferation were significantly upregulated, such as muscle-specific transmembrane fusogenic protein Myomaker (*Mymk*), insulin like growth factor binding protein 5 (*Igfbp5*), Growth differentiation factor 11 (*Gdf11*), and the well-characterized long non-coding RNA H19 Imprinted Maternally Expressed Transcript (*H19*) (Figure 18 & 20). To further evaluate the top significantly upregulated and downregulated genes in response to MYTHO-KD, we employed a gene ontology (GO) analysis of our microarray dataset. The GO analysis of 218 upregulated and 170 downregulated genes ($p < 0.05$) showed marked enrichment of gene sets involved in regulation of cellular response to growth factor stimulus, stem cell differentiation, and myotube differentiation involved in muscle regeneration (Figure 19).

Finally, to elucidate the potential transcription factors regulating the transcriptional changes in response to transfection with siRNA-Mytho oligos, we employed a Transcriptional Regulatory Relationships Unraveled by Sentence-based Text mining (TRRUST) analysis, which identified transcription factors MyoD1 and Myogenin as the top candidates (Figure 21). Further supporting this, an Ingenuity Pathway Analysis (IPA) of differentially expressed genes identified several networks that are transcriptionally regulated by MyoD1 and Myogenin (Figure 22).

Identification of MYTHO interactome

To identify potential proteins that interact with MYTHO across myogenesis, we employed an immunoprecipitation technique combined with mass spectrometry screening of protein-protein interactions in three distinct phases of myogenesis: (1) myoblasts in serum rich medium; (2) myoblasts exposed to low serum conditions for 12 hours; and (3) day 5 myotubes.

As shown in Figure 23A&B, MYTHO interacts with the Septin family (Septin -2, -5, -6, -7, -8, -9, -10, -11), Microtubule associated cell migration factor (BCAS3), and ATPase family AAA domain containing 2 (ATAD2) in myoblasts in serum rich medium and myoblasts exposed to low serum conditions for 12 hours. After 5 days in differentiation medium, the interaction with ATAD2 was not detectable, while the interaction with the Septin family of proteins and BCAS3 remained positive, suggesting that MYTHO may interact with ATAD2 exclusively in myoblasts rather than differentiated myotubes.

SECTION 4: DISCUSSION

The main observations of this study are: 1) MYTHO expression is upregulated during differentiation and has both a nuclear and cytosolic localization during differentiation of myoblasts into myotubes; 2) MYTHO-KD leads to early activation of the myogenic program through induction of transcription factors *MyoD1* and *Myogenin* and late markers of differentiation *MyHC* and *MCK*; 3) MYTHO-- KD leads to hypertrophic myotube formation as indicated by significant increases in fusion and differentiation indices and pro-differentiation genes *Mymk*, *Mymx*, *Igfbp5*, and *Fgf21*; 4) MYTHO-KD reduces the proliferation capacity of myoblasts but does not affect cell cycle distribution; 5) transcriptome profiling of MYTHO-KD myoblasts revealed marked increases in pathways related to muscle growth, differentiation, and development; and finally 6) proteomic screenings of MYTHO-associated proteins indicated that ATAD2, BCAS3, and the Septin family of proteins are probable interactors of MYTHO within the context of myogenesis.

To our knowledge, the current study is the first to examine the functional role of MYTHO during myogenesis. Our investigations address the unmet clinical need for cellular therapies with immediate application in the prevention and potential treatment of diseases associated with loss of skeletal muscle mass and function. Translational research efforts into mechanisms of muscle regeneration continue to face major limitations in identifying and characterizing novel and innovative therapeutic targets. Therefore, the primary motivation of this study was to identify and characterize a novel gene involved in myogenesis with potential for therapeutic application in conditions of loss of skeletal muscle mass and function.

To characterize the expression pattern and localization of MYTHO throughout myogenesis, we measured the mRNA and protein levels and visualized an immunostaining of MYTHO during a differentiation time course. The mRNA and protein levels of MYTHO follow a similar pattern, whereby differentiation induces *Mytho* expression. An

immunostaining of MYTHO revealed a nuclear localization in myoblasts and a nuclear/cytoplasmic localization in myotubes. According to the Human Protein Atlas, the predicted localization of MYTHO is intracellular, where it mainly localizes to the nuclear speckles, nucleoli fibrillar center, and, to a lesser extent, the cytosol [106]. As well, UniprotKB reports localization to the Golgi apparatus <https://www.uniprot.org/uniprot/Q9BSU1>. MYTHO is reported to have over 60 binary interactions [95, 107], In line with Human Protein Atlas reports, our results confirm the nuclear localization of MYTHO in myoblasts, while in myotubes, MYTHO had a nuclear and cytoplasmic localization.

To assess the functional importance of MYTHO in regulating myogenesis, we employed a loss-of-function approach using an RNAiMax-mediated transfection with selective D230025D16-201 siRNA oligos. Using this approach, we achieved a significant reduction in the mRNA and protein levels of MYTHO. While the reduction in MYTHO mRNA and protein levels were only around 50%, we were able to detect differences at the transcriptomic and protein levels between myoblasts transfected with *Mytho* oligos and control oligos, in addition to phenotypical differences. These observations suggest that the use of an RNAi-mediated transfection with siRNA oligos for MYTHO is an appropriate loss-of-function approach to evaluate the functional importance of this gene in regulating myogenesis.

The observation that MYTHO-KD is associated with upregulation of mRNA expression of *MyoD1*, *MyoG*, *MyHC1*, and *MCK* indicates that MYTHO has a potential role in regulating the myogenic program. To evaluate if this effect is detectable at the protein level, we employed an immunofluorescence staining of Myogenin and found a higher percentage of Myogenin positive cells in response to MYTHO KD. Collectively, these results suggest that the presence of MYTHO is necessary for proper induction of the myogenic program, and that a loss-of-function of MYTHO is sufficient to induce early activation of the myogenic program. Acute depletion of MYTHO was sufficient to induce hypertrophic myotubes early in the

differentiation time course, as indicated by significant increase in the fusion and differentiation indices, suggesting that MYTHO may play an important role in regulating the formation and growth of myotubes. To support this finding, we detected an increase in the expression of genes known to promote differentiation and fusion of myoblasts into myotubes (*Mymk*, *Mymx*, *Fgf21*, *Igfbp5*) [76, 80, 108-110]. To evaluate whether MYTHO has a role in myogenesis beyond its effects on myoblast differentiation, we evaluated whether MYTHO-KD is associated with changes in myoblast proliferation. Interestingly, we found that MYTHO-KD resulted in a significant decrease in the proliferation capacity of myoblasts but did not influence the cell cycle. Collectively, these results suggest that MYTHO is a novel regulator of myoblast proliferation, differentiation, and fusion into myotubes. More specifically, the observations reported in the study suggest that MYTHO has a repressive role during myogenesis, specifically by regulating growth and differentiation.

The findings of the present study build on the recent work of Leduc-Gaudet *et al.* (2023), who described the crucial role of MYTHO in regulating growth of adult skeletal muscle [103]. The present study further demonstrates the role played by MYTHO in regulating growth, as we show that MYTHO-KD influences myotube size. To investigate the mechanisms underlying early activation of the myogenic program, accelerated differentiation, and myotube hypertrophy induced by MYTHO KD, we employed a microarray-based transcriptome analysis at 48 hours after transfection with siRNA-Mytho oligos. Interestingly, various pathways were enriched in response to MYTHO KD, such as regulation of cellular response to growth factor stimulus and stem cell differentiation, which suggests that MYTHO may play a regulatory role in these pathways during myogenesis. Furthermore, genes that have previously been reported to be involved in muscle cell growth and development are upregulated in response to MYTHO-KD [111-120], indicating that endogenous expression of MYTHO is important in regulating myogenic commitment to differentiation. Collectively, these observations indicate the

involvement of MYTHO in reprogramming the transcriptome during differentiation, possibly as part of the mechanism underlying muscle cell specification and commitment.

To further explore the potential mechanisms underlying the regulatory role of MYTHO during myogenesis, we employed immunoprecipitation and mass spectral analyses to identify the MYTHO interactome. The proteomic screening revealed possible protein-protein interactions with BCAS3, the Septin family, and ATAD2 proteins. The interaction of MYTHO with BCAS3 was previously reported in other studies, thereby confirming the accuracy of our proteomic screening [94, 98]. This study is the first to report an interaction between MYTHO and BCAS3 in myoblasts and myotubes, which suggests that this interaction may be conserved across different cell types and states. BCAS3 has a well-characterized role in breast cancer progression [121, 122], cardiovascular development [123, 124], and has even been reported to cause a neurodevelopmental disorder when loss-of-function mutations occur in humans [125]. However, the role of BCAS3 in the regulation of myogenesis has never been studied. Therefore, the interaction of MYTHO and BCAS3 requires further examination in order to identify a potential regulatory partnership during myogenesis.

The Septin family is regarded as the fourth element of the cytoskeleton [126, 127], with diverse roles such as regulation of cell shape, cell migration, vesicle trafficking, and receptor signaling [128, 129]. Recent observations from Gönczi and colleagues reveal the novel role of Septin 7 in the regulation of skeletal muscle architecture and morphology, including adult myofibers and C2C12 myoblasts [130]. Indeed, Gönczi and colleagues report that knockdown of Septin7 in C2C12 cells resulted in improper myoblast differentiation and fusion into myotubes, suggesting a novel role for Septin7 in the regulation of myogenesis. Recently, Septin 7 was reported to interact with Numb, a well-characterized regulator of Notch signaling and cell fate [131, 132], in C2C12 myotubes [133]. Numb has previously been reported to play a role in the regulation of skeletal muscle contraction [134], satellite cell proliferation during

muscle regeneration [135], and the formation of a complex with MyoD1 during nandrolone treatment [136]. In addition to interacting with Septin 7, liquid chromatography (LC)/mass spectrometry (MS)/MS analysis performed by Gasperi *et al.* (2023) also indicated a potential interaction of Numb with Septin 2, 9, and 10 [133], suggesting that Numb may form a complex with the Septin family. As such, the interaction of MYTHO and Septin7 requires further examination in order to identify a potential regulatory partnership during myogenesis.

The protein-protein interaction between ATAD2 and MYTHO was not detected after 5 days of differentiation was ATAD2, but the association of these proteins was detected in myoblasts, indicating a potential partnership between MYTHO and ATAD2 in the regulation of early myogenesis. ATAD2, which stands for ATPase Family AAA Domain Containing 2, has been characterized as a transcriptional co-activator and epigenetic reader of newly synthesized histone di-acetylation-marks during DNA replication [137]. The function of ATAD2 is well-characterized in cancer as it has been described as an oncogene capable of reprogramming the genome in the context of malignant cell transformation and cancer aggressiveness [138, 139]. While there are currently no studies on the role of ATAD2 within the context of myogenesis, data mining analyses reveal that ATAD2 may be involved in satellite cell activation and proliferation as microarray data from day 3 cardiotoxin-injury samples reveal ATAD2 is among the top differentially expressed genes [140]. This indicates that ATAD2 could potentially be involved in early stages of myogenesis, during satellite cell activation, myoblast proliferation, and possibly in preparing myoblasts for proper differentiation and fusion. Indeed, according to CycleBase ATAD2 is in the top 20 genes expressed in the S phase (DNA replication) of cell cycle [141], indicating that it may prepare the genomic landscape to cope with the demands of differentiation. Interestingly, ATAD2 was identified as one of the top progressively up-regulated genes during dedifferentiation (i.e., transient process by which cells become less specialized and return to an earlier cell state within

the same lineage) [142]. The interaction between MYTHO and ATAD2 within the regulation of satellite cell activation, proliferation, and differentiation warrants further investigation.

In summary, this study characterized MYTHO as a novel regulator of proliferation, differentiation, and fusion of myoblasts into myotubes. MYTHO knockdown is indeed sufficient to induce early commitment to the myogenic program and cause formation of hypertrophic myotubes. Whether MYTHO is involved in the process of satellite cell activation, proliferation, differentiation, and fusion into adult skeletal muscle fibers *in vivo* will require further studies. Our observations lay the groundwork for future research into the novel mechanisms by which MYTHO regulates muscle regeneration. Understanding the role of MYTHO throughout the different phases of myogenesis and the proteins involved in this pathway will have a major impact on identification of innovative therapeutic targets for prevention and potential treatment of loss of skeletal muscle mass and function associated with aging, injury, and disease. Since the role of MYTHO in contributing to the pathophysiology of disease is unknown, there is a novel opportunity to leverage the growing understanding of MYTHO for identification of diseases associated with pathways in which MYTHO is involved. Toward this end, we propose that MYTHO is a novel regulator of myogenesis that should be further characterized in pre-clinical models.

SECTION 5: REFERENCES

1. Mukund, K. and S. Subramaniam, *Skeletal muscle: A review of molecular structure and function, in health and disease*. Wiley Interdiscip Rev Syst Biol Med, 2020. **12**(1): p. e1462.
2. Talbot, J. and L.J.W.I.R.D.B. Maves, *Skeletal muscle fiber type: using insights from muscle developmental biology to dissect targets for susceptibility and resistance to muscle disease*. 2016. **5**(4): p. 518-534.
3. Radák, Z., *The physiology of physical training*. 2018: Academic Press.
4. Hopkins, P.M.J.C.E.i.A., *Critical Care and Pain, Skeletal muscle physiology*. 2006. **6**(1): p. 1-6.
5. Nishimaru, H., et al., *Mammalian motor neurons corelease glutamate and acetylcholine at central synapses*. Proc Natl Acad Sci U S A, 2005. **102**(14): p. 5245-9.
6. Baylor, S.M. and S. Hollingworth, *Calcium indicators and calcium signalling in skeletal muscle fibres during excitation-contraction coupling*. Prog Biophys Mol Biol, 2011. **105**(3): p. 162-79.
7. Rowe, R.W., *Ultrastructure of the Z line of skeletal muscle fibers*. J Cell Biol, 1971. **51**(3): p. 674-85.
8. Rall, J.A., *Energetic aspects of skeletal muscle contraction: implications of fiber types*. Exerc Sport Sci Rev, 1985. **13**: p. 33-74.

9. Wolfe, R.R., *The underappreciated role of muscle in health and disease*. Am J Clin Nutr, 2006. **84**(3): p. 475-82.
10. Frontera, W.R. and J. Ochala, *Skeletal muscle: a brief review of structure and function*. Calcif Tissue Int, 2015. **96**(3): p. 183-95.
11. Sartori, R., V. Romanello, and M. Sandri, *Mechanisms of muscle atrophy and hypertrophy: implications in health and disease*. Nat Commun, 2021. **12**(1): p. 330.
12. Schiaffino, S., et al., *Mechanisms regulating skeletal muscle growth and atrophy*. FEBS J, 2013. **280**(17): p. 4294-314.
13. Hoppeler, H. and M. Flück, *Normal mammalian skeletal muscle and its phenotypic plasticity*. J Exp Biol, 2002. **205**(Pt 15): p. 2143-52.
14. Christensen, J., et al., *Muscle dysfunction in cancer patients*. J Annals of Oncology, 2014. **25**(5): p. 947-958.
15. Kim, H.C., M. Mofarrahi, and S.N. Hussain, *Skeletal muscle dysfunction in patients with chronic obstructive pulmonary disease*. International journal of chronic obstructive pulmonary disease, 2008. **3**(4): p. 637.
16. Park, S.W., et al., *Accelerated loss of skeletal muscle strength in older adults with type 2 diabetes: the health, aging, and body composition study*. Diabetes care, 2007. **30**(6): p. 1507-1512.
17. Suzuki, T., S. Palus, and J. Springer, *Skeletal muscle wasting in chronic heart failure*. ESC heart failure, 2018. **5**(6): p. 1099-1107.

18. Avin, K.G., et al., *Skeletal muscle regeneration and oxidative stress are altered in chronic kidney disease*. PLoS One, 2016. **11**(8): p. e0159411.
19. Suetta, C., et al., *Ageing is associated with diminished muscle re-growth and myogenic precursor cell expansion early after immobility-induced atrophy in human skeletal muscle*. The Journal of physiology, 2013. **591**(15): p. 3789-3804.
20. Hussain, S.N., *Respiratory muscle dysfunction in sepsis*. Molecular and Cellular Biochemistry, 1998. **179**(1-2): p. 125-134.
21. Wens, I., et al., *Multiple sclerosis affects skeletal muscle characteristics*. PloS one, 2014. **9**(9): p. e108158.
22. Preedy, V., et al., *Alcoholic skeletal muscle myopathy: definitions, features, contribution of neuropathy, impact and diagnosis*. European Journal of Neurology, 2001. **8**(6): p. 677-687.
23. Hurley, M.V., *The role of muscle weakness in the pathogenesis of osteoarthritis*. Rheumatic disease clinics of North America, 1999. **25**(2): p. 283-298.
24. Emery, A.E., F. Muntoni, and R.C. Quinlivan, *Duchenne muscular dystrophy*. 2015: OUP Oxford.
25. Papa, E.V., X. Dong, and M. Hassan, *Skeletal Muscle Function Deficits in the Elderly: Current Perspectives on Resistance Training*. J Nat Sci, 2017. **3**(1).

26. Cruz-Jentoft, A.J. and A.A. Sayer, *Sarcopenia*. Lancet, 2019. **393**(10191): p. 2636-2646.
27. Janssen I, S.D., Katzmarzyk PT, Roubenoff R *The healthcare costs of sarcopenia in the United States*. Journal of American Geriatric Society, 2004. **52**(1): p. 80-5.
28. Hanna, L., et al., *Association between skeletal muscle mass and quality of life in adults with cancer: a systematic review and meta-analysis*. J Cachexia Sarcopenia Muscle, 2022. **13**(2): p. 839-857.
29. Sobestiansky, S., K. Michaelsson, and T. Cederholm, *Sarcopenia prevalence and associations with mortality and hospitalisation by various sarcopenia definitions in 85-89 year old community-dwelling men: a report from the ULSAM study*. BMC Geriatr, 2019. **19**(1): p. 318.
30. Beaudart, C., et al., *Quality of life in sarcopenia measured with the SarQoL®: impact of the use of different diagnosis definitions*. Aging Clin Exp Res, 2018. **30**(4): p. 307-313.
31. Beaudart, C., et al., *Current review of the SarQoL®: a health-related quality of life questionnaire specific to sarcopenia*. Expert Rev Pharmacoecon Outcomes Res, 2017. **17**(4): p. 335-341.

32. Artero, E.G., et al., *A prospective study of muscular strength and all-cause mortality in men with hypertension*. J Am Coll Cardiol, 2011. **57**(18): p. 1831-7.
33. Newman, A.B., et al., *Strength, but not muscle mass, is associated with mortality in the health, aging and body composition study cohort*. J Gerontol A Biol Sci Med Sci, 2006. **61**(1): p. 72-7.
34. Katzmarzyk, P.T. and C.L. Craig, *Musculoskeletal fitness and risk of mortality*. Med Sci Sports Exerc, 2002. **34**(5): p. 740-4.
35. Ruiz, J.R., et al., *Association between muscular strength and mortality in men: prospective cohort study*. Bmj, 2008. **337**(7661): p. a439.
36. Steffl, M., et al., *The increase in health care costs associated with muscle weakness in older people without long-term illnesses in the Czech Republic: results from the Survey of Health, Ageing and Retirement in Europe (SHARE)*. Clin Interv Aging, 2017. **12**: p. 2003-2007.
37. Pinedo-Villanueva, R., et al., *Health Care Costs Associated With Muscle Weakness: A UK Population-Based Estimate*. Calcif Tissue Int, 2019. **104**(2): p. 137-144.
38. Beaudart, C., et al., *Sarcopenia: burden and challenges for public health*. Arch Public Health, 2014. **72**(1): p. 45.

39. Janssen, I., et al., *The healthcare costs of sarcopenia in the United States*. J Am Geriatr Soc, 2004. **52**(1): p. 80-5.
40. Chaput, J.P., et al., *Economic burden of low muscle strength in Canadian adults*. Appl Physiol Nutr Metab, 2023.
41. Canada, G.o., *Action for Seniors Report*. 2014.
42. Canada, S., *Census in Brief: A portrait of the population aged 85 and older in 2016 in Canada*, C.C. Program, Editor. 2017.
43. Judson, R.N. and F.M. Rossi, *Towards stem cell therapies for skeletal muscle repair*. npj Regenerative Medicine, 2020. **5**(1): p. 1-6.
44. Tedesco, F.S., et al., *Repairing skeletal muscle: regenerative potential of skeletal muscle stem cells*. J Clin Invest, 2010. **120**(1): p. 11-9.
45. Yusuf, F. and B. Brand-Saberi, *Myogenesis and muscle regeneration*. Histochem Cell Biol, 2012. **138**(2): p. 187-99.
46. Chargé, S.B. and M.A. Rudnicki, *Cellular and molecular regulation of muscle regeneration*. Physiol Rev, 2004. **84**(1): p. 209-38.
47. Péault, B., et al., *Stem and progenitor cells in skeletal muscle development, maintenance, and therapy*. Mol Ther, 2007. **15**(5): p. 867-77.
48. Garry, G.A., M.L. Antony, and D.J. Garry, *Cardiotoxin Induced Injury and Skeletal Muscle Regeneration*. Methods Mol Biol, 2016. **1460**: p. 61-71.

49. Mahdy, M.A.A., *Glycerol-induced injury as a new model of muscle regeneration*. Cell Tissue Res, 2018. **374**(2): p. 233-241.
50. Sambasivan, R., et al., *Pax7-expressing satellite cells are indispensable for adult skeletal muscle regeneration*. J Development, 2011. **138**(17): p. 3647-3656.
51. Mauro, A.J.T.J.o.b. and b. cytology, *Satellite cell of skeletal muscle fibers*. 1961. **9**(2): p. 493.
52. Yin, H., F. Price, and M.A. Rudnicki, *Satellite cells and the muscle stem cell niche*. Physiol Rev, 2013. **93**(1): p. 23-67.
53. Dumont, N.A., et al., *Satellite Cells and Skeletal Muscle Regeneration*. Compr Physiol, 2015. **5**(3): p. 1027-59.
54. Fu, X., H. Wang, and P. Hu, *Stem cell activation in skeletal muscle regeneration*. J Cellular and Molecular Life Sciences 2015. **72**(9): p. 1663-1677.
55. Snow, M.H., *Myogenic cell formation in regenerating rat skeletal muscle injured by mincing II. An autoradiographic study*. The Anatomical Record, 1977. **188**(2): p. 201-217.
56. Conlon, I. and M. Raff, *Size control in animal development*. Cell, 1999. **96**(2): p. 235-44.

57. Chakravarthy, M.V., B.S. Davis, and F.W. Booth, *IGF-I restores satellite cell proliferative potential in immobilized old skeletal muscle*. Journal of Applied Physiology, 2000. **89**(4): p. 1365-1379.
58. Machida, S., E.E. Spangenburg, and F.W. Booth, *Forkhead transcription factor FoxO1 transduces insulin-like growth factor's signal to p27Kip1 in primary skeletal muscle satellite cells*. Journal of cellular physiology, 2003. **196**(3): p. 523-531.
59. Nadal-Ginard, B., *Commitment, fusion and biochemical differentiation of a myogenic cell line in the absence of DNA synthesis*. Cell, 1978. **15**(3): p. 855-864.
60. Clegg, C.H., et al., *Growth factor control of skeletal muscle differentiation: commitment to terminal differentiation occurs in G1 phase and is repressed by fibroblast growth factor*. The Journal of cell biology, 1987. **105**(2): p. 949-956.
61. Bartek, J., J. Bartkova, and J. Lukas, *The retinoblastoma protein pathway and the restriction point*. Current opinion in cell biology, 1996. **8**(6): p. 805-814.
62. Lukas, J., J. Bartkova, and J. Bartek, *Convergence of mitogenic signalling cascades from diverse classes of receptors at the cyclin D-cyclin-dependent kinase-pRb-controlled G1 checkpoint*. J Molecular cellular biology

1996. **16**(12): p. 6917-6925.

63. Johnson, D. and C. Walker, *Cyclins and cell cycle checkpoints*. J Annual review of pharmacology toxicology

1999. **39**.

64. Sun, L., et al., *JAK1-STAT1-STAT3, a key pathway promoting proliferation and preventing premature differentiation of myoblasts*. Journal of cell biology, 2007. **179**(1): p. 129-138.

65. Fujio, Y., et al., *Cell cycle withdrawal promotes myogenic induction of Akt, a positive modulator of myocyte survival*. Mol Cell Biol, 1999. **19**(7): p. 5073-82.

66. Skapek, S.X., et al., *Inhibition of myogenic differentiation in proliferating myoblasts by cyclin D1-dependent kinase*. 1995. **267**(5200): p. 1022-1024.

67. Walsh, K. and H. Perlman, *Cell cycle exit upon myogenic differentiation*. Curr Opin Genet Dev, 1997. **7**(5): p. 597-602.

68. Barr, A.R., et al., *DNA damage during S-phase mediates the proliferation-quiescence decision in the subsequent G1 via p21 expression*. Nature communications, 2017. **8**(1): p. 1-17.

69. Yaffe, D., *Cellular aspects of muscle differentiation in vitro*, in *Current topics in developmental biology*. 1969, Elsevier. p. 37-77.

70. Konigsberg, I.R., *Clonal analysis of myogenesis*. Science, 1963. **140**(3573): p. 1273-1284.
71. Odorico, J.S., D.S. Kaufman, and J.A. Thomson, *Multilineage differentiation from human embryonic stem cell lines*. Stem Cells, 2001. **19**(3): p. 193-204.
72. Zhang, K., J. Sha, and M.L. Harter, *Activation of Cdc6 by MyoD is associated with the expansion of quiescent myogenic satellite cells*. Journal of Cell Biology, 2010. **188**(1): p. 39-48.
73. Megeney, L.A., et al., *MyoD is required for myogenic stem cell function in adult skeletal muscle*. 1996. **10**(10): p. 1173-1183.
74. Hasty, P., et al., *Muscle deficiency and neonatal death in mice with a targeted mutation in the myogenin gene*. Nature, 1993. **364**(6437): p. 501-506.
75. Davis, R.L., H. Weintraub, and A.B. Lassar, *Expression of a single transfected cDNA converts fibroblasts to myoblasts*. Cell, 1987. **51**(6): p. 987-1000.
76. Millay, D.P., et al., *Myomaker is a membrane activator of myoblast fusion and muscle formation*. Nature, 2013. **499**(7458): p. 301-5.
77. Zhang, H., et al., *Human myotube formation is determined by MyoD-Myomixer/Myomaker axis*. Science Advances, 2020. **6**(51): p. eabc4062.

78. Leikina, E., et al., *Myomaker and Myomerger Work Independently to Control Distinct Steps of Membrane Remodeling during Myoblast Fusion*. Dev Cell, 2018. **46**(6): p. 767-780.e7.
79. Quinn, M.E., et al., *Myomerger induces fusion of non-fusogenic cells and is required for skeletal muscle development*. Nat Commun, 2017. **8**: p. 15665.
80. Bi, P., et al., *Control of muscle formation by the fusogenic micropeptide myomixer*. Science, 2017. **356**(6335): p. 323-327.
81. Zhang, Q., et al., *The microprotein Minion controls cell fusion and muscle formation*. Nat Commun, 2017. **8**: p. 15664.
82. Camarda, G., et al., *A pRb-independent mechanism preserves the postmitotic state in terminally differentiated skeletal muscle cells*. The Journal of cell biology, 2004. **167**(3): p. 417-423.
83. Buckingham, M. and E. Tzahor, *In remembrance of David Yaffe*. Skelet Muscle, 2020. **10**(1): p. 31.
84. Yaffe, D. and O. Saxel, *Serial passaging and differentiation of myogenic cells isolated from dystrophic mouse muscle*. Nature, 1977. **270**(5639): p. 725-7.
85. Yablonka-Reuveni, Z., et al., *Farewell to Professor David Yaffe - A pillar of the myogenesis field*. Eur J Transl Myol, 2020. **30**(3): p. 9306.

86. Rajan, S., et al., *Analysis of early C2C12 myogenesis identifies stably and differentially expressed transcriptional regulators whose knock-down inhibits myoblast differentiation*. *Physiol Genomics*, 2012. **44**(2): p. 183-97.
87. Burattini, S., et al., *C2C12 murine myoblasts as a model of skeletal muscle development: morpho-functional characterization*. *Eur J Histochem*, 2004. **48**(3): p. 223-33.
88. Dey, B.K., et al., *miR-26a is required for skeletal muscle differentiation and regeneration in mice*. *Genes Dev*, 2012. **26**(19): p. 2180-91.
89. Han, H., *RNA Interference to Knock Down Gene Expression*. *Methods Mol Biol*, 2018. **1706**: p. 293-302.
90. Milan, G., et al., *Regulation of autophagy and the ubiquitin–proteasome system by the FoxO transcriptional network during muscle atrophy*. *Nature communications*, 2015. **6**(1): p. 1-14.
91. Schapira, M., et al., *WD40 repeat domain proteins: a novel target class?* *Nature reviews Drug discovery*, 2017. **16**(11): p. 773.
92. Stirnimann, C.U., et al., *WD40 proteins propel cellular networks*. *Trends in biochemical sciences*, 2010. **35**(10): p. 565-574.
93. Birgisdottir, Å.B., T. Lamark, and T. Johansen, *The LIR motif–crucial for selective autophagy*. *Journal of cell science*, 2013. **126**(15): p. 3237-3247.

94. Yamada, Y. and P. Schaap, *The proppin bcas3 and its interactor kinkyA localize to the early phagophore and regulate autophagy*. *Autophagy*, 2020: p. 1-16.
95. Huttlin, E.L., et al., *Architecture of the human interactome defines protein communities and disease networks*. *Nature*, 2017. **545**(7655): p. 505-509.
96. Rolland, T., et al., *A proteome-scale map of the human interactome network*. *Cell*, 2014. **159**(5): p. 1212-1226.
97. Fragoza, R., et al., *Extensive disruption of protein interactions by genetic variants across the allele frequency spectrum in human populations*. *Nature communications*, 2019. **10**(1): p. 1-15.
98. Kojima, W., et al., *Mammalian BCAS3 and C16orf70 associate with the phagophore assembly site in response to selective and non-selective autophagy*. *Autophagy*, 2021: p. 1-26.
99. Lim, J., et al., *A protein-protein interaction network for human inherited ataxias and disorders of Purkinje cell degeneration*. *Cell*, 2006. **125**(4): p. 801-14.
100. Petrakis, S., et al., *Identification of human proteins that modify misfolding and proteotoxicity of pathogenic ataxin-1*. *PLoS Genet*, 2012. **8**(8): p. e1002897.

101. Haenig, C., et al., *Interactome mapping provides a network of neurodegenerative disease proteins and uncovers widespread protein aggregation in affected brains*. Cell Reports, 2020. **32**(7): p. 108050.
102. Rukova, B., et al., *Whole genome methylation analyses of schizophrenia patients before and after treatment*. Biotechnology Biotechnological Equipment, 2014. **28**(3): p. 518-524.
103. Leduc-Gaudet, J.-P., et al., *MYTHO is a novel regulator of skeletal muscle autophagy and integrity*. Nature Communications, 2023. **14**(1): p. 1199.
104. Ritchie, M.E., et al., *limma powers differential expression analyses for RNA-sequencing and microarray studies*. Nucleic acids research, 2015. **43**(7): p. e47-e47.
105. Zhou, Y., et al., *Metascape provides a biologist-oriented resource for the analysis of systems-level datasets*. Nature communications, 2019. **10**(1): p. 1-10.
106. Uhlén, M., et al., *Tissue-based map of the human proteome*. Science, 2015. **347**(6220).
107. Luck, K., et al., *A reference map of the human binary protein interactome*. Nature, 2020. **580**(7803): p. 402-408.

108. Liu, X., et al., *Fibroblast Growth Factor 21 Promotes C2C12 Cells Myogenic Differentiation by Enhancing Cell Cycle Exit*. Biomed Res Int, 2017. **2017**: p. 1648715.
109. Ren, H., P. Yin, and C. Duan, *IGFBP-5 regulates muscle cell differentiation by binding to IGF-II and switching on the IGF-II auto-regulation loop*. The Journal of cell biology, 2008. **182**(5): p. 979-991.
110. Cobb, L.J., et al., *Partitioning of IGFBP-5 actions in myogenesis: IGF-independent anti-apoptotic function*. J Cell Sci, 2004. **117**(Pt 9): p. 1737-46.
111. Tomczak, K.K., et al., *Expression profiling and identification of novel genes involved in myogenic differentiation*. Faseb j, 2004. **18**(2): p. 403-5.
112. Do, M.K., et al., *Growth factor regulation of neural chemorepellent Sema3A expression in satellite cell cultures*. Am J Physiol Cell Physiol, 2011. **301**(5): p. C1270-9.
113. Henningsen, J., et al., *Dynamics of the skeletal muscle secretome during myoblast differentiation*. Mol Cell Proteomics, 2010. **9**(11): p. 2482-96.
114. Dey, B.K., K. Pfeifer, and A. Dutta, *The H19 long noncoding RNA gives rise to microRNAs miR-675-3p and miR-675-5p to promote skeletal*

- muscle differentiation and regeneration*. Genes Dev, 2014. **28**(5): p. 491-501.
115. Cai, A., et al., *Myogenic differentiation of human myoblasts and Mesenchymal stromal cells under GDF11 on NPoly- ϵ -caprolactone-collagen I-Polyethylene-nanofibers*. BMC Mol Cell Biol, 2023. **24**(1): p. 18.
116. Sharples, A.P., et al., *The role of insulin-like-growth factor binding protein 2 (IGFBP2) and phosphatase and tensin homologue (PTEN) in the regulation of myoblast differentiation and hypertrophy*. Growth Horm IGF Res, 2013. **23**(3): p. 53-61.
117. Li, Y., et al., *Decorin gene transfer promotes muscle cell differentiation and muscle regeneration*. Mol Ther, 2007. **15**(9): p. 1616-22.
118. Kishioka, Y., et al., *Decorin enhances the proliferation and differentiation of myogenic cells through suppressing myostatin activity*. J Cell Physiol, 2008. **215**(3): p. 856-67.
119. Yang, L., et al., *MiR-452 Regulates C2C12 Myoblast Proliferation and Differentiation via Targeting ANGPT1*. Front Genet, 2021. **12**: p. 640807.
120. Mofarrahi, M., et al., *Angiopoietin-1 enhances skeletal muscle regeneration in mice*. Am J Physiol Regul Integr Comp Physiol, 2015. **308**(7): p. R576-89.

121. Zhou, Z., et al., *BCAS3 exhibits oncogenic properties by promoting CRL4A-mediated ubiquitination of p53 in breast cancer*. *Cell Prolif*, 2021. **54**(8): p. e13088.
122. Bärlund, M., et al., *Cloning of BCAS3 (17q23) and BCAS4 (20q13) genes that undergo amplification, overexpression, and fusion in breast cancer*. *Genes Chromosomes Cancer*, 2002. **35**(4): p. 311-7.
123. Siva, K., et al., *Human BCAS3 expression in embryonic stem cells and vascular precursors suggests a role in human embryogenesis and tumor angiogenesis*. *PLoS One*, 2007. **2**(11): p. e1202.
124. Shetty, R., et al., *Rudhira/BCAS3 is essential for mouse development and cardiovascular patterning*. *Scientific Reports*, 2018. **8**.
125. Hengel, H., et al., *Bi-allelic loss-of-function variants in BCAS3 cause a syndromic neurodevelopmental disorder*. *Am J Hum Genet*, 2021. **108**(6): p. 1069-1082.
126. Mostowy, S. and P. Cossart, *Septins: the fourth component of the cytoskeleton*. *Nat Rev Mol Cell Biol*, 2012. **13**(3): p. 183-94.
127. Dolat, L., Q. Hu, and E.T. Spiliotis, *Septin functions in organ system physiology and pathology*. *Biol Chem*, 2014. **395**(2): p. 123-41.
128. Ivanov, A.I., et al., *Novel Functions of the Septin Cytoskeleton: Shaping Up Tissue Inflammation and Fibrosis*. *Am J Pathol*, 2021. **191**(1): p. 40-51.

129. Gönczi, M., et al., *Septins, a cytoskeletal protein family, with emerging role in striated muscle*. J Muscle Res Cell Motil, 2021. **42**(2): p. 251-265.
130. Gönczi, M., et al., *Septin7 is indispensable for proper skeletal muscle architecture and function*. Elife, 2022. **11**.
131. Gulino, A., L. Di Marcotullio, and I. Screpanti, *The multiple functions of Numb*. Exp Cell Res, 2010. **316**(6): p. 900-6.
132. Beres, B.J., et al., *Numb regulates Notch1, but not Notch3, during myogenesis*. Mech Dev, 2011. **128**(5-6): p. 247-57.
133. Gasperi, R.D., et al., *SEPTIN 7 INTERACTS WITH NUMB TO PRESERVE SARCOMERE STRUCTURAL ORGANIZATION AND MUSCLE CONTRACTILE FUNCTION*. bioRxiv, 2023: p. 2023.05.11.540467.
134. De Gasperi, R., et al., *Numb is required for optimal contraction of skeletal muscle*. J Cachexia Sarcopenia Muscle, 2022. **13**(1): p. 454-466.
135. George, R.M., et al., *Numb-deficient satellite cells have regeneration and proliferation defects*. Proc Natl Acad Sci U S A, 2013. **110**(46): p. 18549-54.
136. Liu, X.H., et al., *Nandrolone-induced nuclear accumulation of MyoD protein is mediated by Numb, a Notch inhibitor, in C2C12 myoblasts*. Physiol Rep, 2018. **6**(1).

137. Koo, S.J., et al., *ATAD2 is an epigenetic reader of newly synthesized histone marks during DNA replication*. *Oncotarget*, 2016. **7**(43): p. 70323-70335.
138. Boussouar, F., et al., *Malignant genome reprogramming by ATAD2*. *Biochim Biophys Acta*, 2013. **1829**(10): p. 1010-4.
139. Nayak, A., M. Dutta, and A. Roychowdhury, *Emerging oncogene ATAD2: Signaling cascades and therapeutic initiatives*. *Life Sci*, 2021. **276**: p. 119322.
140. Zhang, L., et al., *Role of integrin- β 3 protein in macrophage polarization and regeneration of injured muscle*. *J Biol Chem*, 2012. **287**(9): p. 6177-86.
141. Liu, Z., et al., *Reconstructing cell cycle pseudo time-series via single-cell transcriptome data*. *Nat Commun*, 2017. **8**(1): p. 22.
142. Yagi, M., et al., *Dissecting dual roles of MyoD during lineage conversion to mature myocytes and myogenic stem cells*. *Genes Dev*, 2021. **35**(17-18): p. 1209-1228.
143. Zhang, Y., *I-TASSER server for protein 3D structure prediction*. *BMC Bioinformatics*, 2008. **9**(40).

SECTION 6: TABLES

Table 1. List of primers used for RT-qPCR.

Gene	Forward primer (5'-3')	Reverse primer (3'-5')
<i>18S</i>	TGCGGTTTAGCGTCGGTGTC	CCAAGTGGCCAAAGCGTA
<i>Mytho</i>	CGCTCCTACCATTGAGCAAA	CCTCGGAAGTTGAGGTGGAA
<i>CyclinA1</i>	ATGATCTCCCCTGCCTCAGC	CCTGCTGATGTGGCCAATGAG
<i>CyclinD1</i>	TGACTGCCGAGAAGTTGTGC	CTCATCCGCCTCTGGCATT
<i>CyclinE1</i>	CCGTCTTGAATTGGGGCAATA	GAGCTTATAGACTTCGCACACC
<i>Fgf21</i>	TCCTGGGTGTCAAAGCCTCT	ATCCTGGTTTGGGGAGTCCT
<i>Igfbp5</i>	AAGAGCTACGGCGAGCAAAC	CAGCTTCTTTCTGCGGTCCT
<i>GAPDH</i>	AAGAAGGTGGTGAAGCAGGCG	ACCAGGAAATGAGCTTGACAA
<i>MCK</i>	ACGAGAACCTCAAGGGTGGA	CACGGACAGCTTCTCCACTG
<i>MyHC</i>	CTTTGCTTACGTCAGTCAAGGT	AGCGCCTGTGAGCTTGTAAG
<i>MyoD1</i>	TCTCTGCTCCTTTGCCACAA	AGTGCTCTTCGGGTTTCAGG
<i>Myogenin</i>	GCACTGGAGTTCGGTCCCAA	TATCCTCCACCGTGATGCTG
<i>Myomaker</i>	CAAACCTGCTCCTGCCTACCC	GGGAGAACGCCACAAAGAAC
<i>Myomixer</i>	AGGCTCTGCTGAGCTGTCTG	GGCCCAATCTCTCCTTCCTC

Table 2. List of antibodies used for immunoblotting and immunofluorescence staining.

Antibody	Source/Product no.	Dilution
Mouse anti MF20 (MyHC)	DSHB AB_2147781	2 μ g/mL
Goat anti-mouse IgG	ThermoFisher F-2761	1:300
Rabbit anti-C16orf70	ThermoFisher PA5-59483	1:100
Recombinant Anti-C16orf70	Abcam ab181987	1:1000
Goat anti Rabbit IgG	Abcam #ab6721	1:5000

SECTION 7: FIGURES

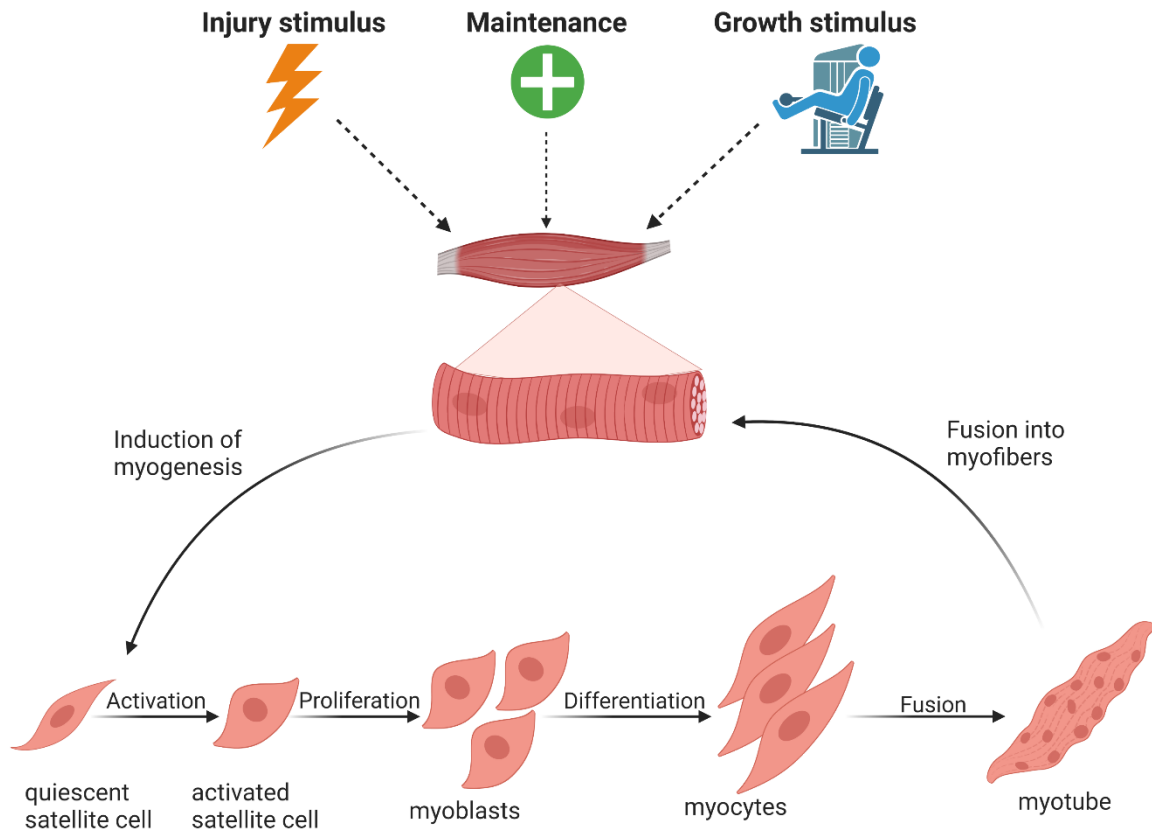


FIGURE 1

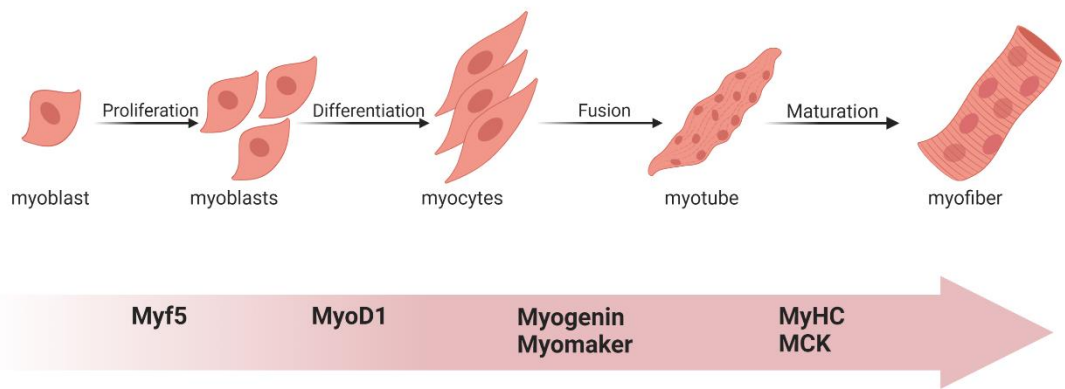


FIGURE 2

```

MOUSE/1-422 1 MLDLEVVPERSLGNEQWEFTLGMP LAQAVAILQKHCRII .NVQVLYSEQSFLSHDLILNL
HUMAN/1-422 1 MLDLEVVPERSLGNEQWEFTLGMP LAQAVAILQKHCRII .NVQVLYSEQSFLSHDLILNL
RAT/1-422 1 MLDLEVVPERSLGNEQWEFTLGMP LAQAVAILQKHCRII .NVQVLYSEQSFLSHDLILNL
1 5 10 15 20 25 30 35 40 45 50 55 60

MOUSE/1-422 61 TQDGI T L F D A F N Q R L K V I E V . # L T K V K L K Y C G V H F N S Q A I A R T I E Q I D Q S F G A T H P G V Y
HUMAN/1-422 61 TQDGI K L F D A F N Q R L K V I E V C D L T K V K L K Y C G V H F N S Q A I A R T I E Q I D Q S F G A T H P G V Y
RAT/1-422 61 TQDGI K L F D A F N Q R L K V I E V Y D L T K V K L K Y C G V H F N S Q A I A R T I E Q I D Q S F G A T H P G V Y
65 70 75 80 85 90 95 100 105 110 115 120

MOUSE/1-422 121 NSAEQLFHLNFRGLSFSFQLDSWTEAPKYEENFAHGLASLQIPHGATVKRMYIYSNSLQ
HUMAN/1-422 121 NSAEQLFHLNFRGLSFSFQLDSWTEAPKYEENFAHGLASLQIPHGATVKRMYIYSNSLQ
RAT/1-422 121 NSAEQLFHLNFRGLSFSFQLDSWTEAPKYEENFAHGLASLQIPHGATVKRMYIYSNSLQ
125 130 135 140 145 150 155 160 165 170 175 180

MOUSE/1-422 181 DTKAPVMSLSCFLGNVYAESVDVLRDGTGPFGLRLRLLAAGCGPGVLADAKMRVFERAVY
HUMAN/1-422 181 DTKAPVMSLSCFLGNVYAESVDVLRDGTGPFGLRLRLLAAGCGPGVLADAKMRVFERAVY
RAT/1-422 181 DTKAPVMSLSCFLGNVYAESVDVLRDGTGPFGLRLRLLAAGCGPGVLADAKMRVFERAVY
185 190 195 200 205 210 215 220 225 230 235 240

MOUSE/1-422 241 FGDSCQDVLISMLGSPHKVFYKSEDKMKIHSPSPHKQVPSKCNDFYFNFTLGVDILFDAN
HUMAN/1-422 241 FGDSCQDVLISMLGSPHKVFYKSEDKMKIHSPSPHKQVPSKCNDFYFNFTLGVDILFDAN
RAT/1-422 241 FGDSCQDVLISMLGSPHKVFYKSEDKMKIHSPSPHKQVPSKCNDFYFNFTLGVDILFDAN
245 250 255 260 265 270 275 280 285 290 295 300

MOUSE/1-422 301 TRKVKKPVLLHTNYPGHYFNFIYHRCEFKIPLAIKKENACGQTEICTTYSKWDSTIQELLGH
HUMAN/1-422 301 TRKVKKPVLLHTNYPGHYFNFIYHRCEFKIPLAIKKENACGQTEICTTYSKWDNIQELLGH
RAT/1-422 301 TRKVKKPVLLHTNYPGHYFNFIYHRCEFKIPLAIKKENACGQTEICTTYSKWDSTIQELLGH
305 310 315 320 325 330 335 340 345 350 355 360

MOUSE/1-422 361 PVEKPVVLRHSSSPNNTNPFESTFCFGLQRMIFEVMQNNHIASVTLYGPPRPGALHRTAE
HUMAN/1-422 361 PVEKPVVLRHSSSPNNTNPFESTFCFGLQRMIFEVMQNNHIASVTLYGPPRPGALHRTAE
RAT/1-422 361 PVEKPVVLRHSSSPNNTNPFESTFCFGLQRMIFEVMQNNHIASVTLYGPPRPGALHRTAE
365 370 375 380 385 390 395 400 405 410 415 420

MOUSE/1-422 421 LP
HUMAN/1-422 421 LP
RAT/1-422 421 LP
LP

```

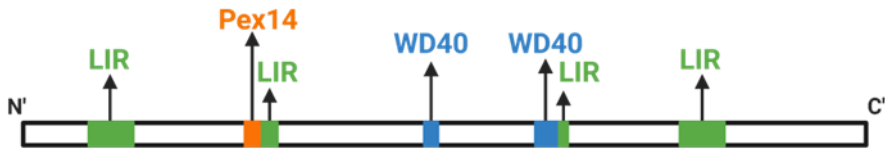
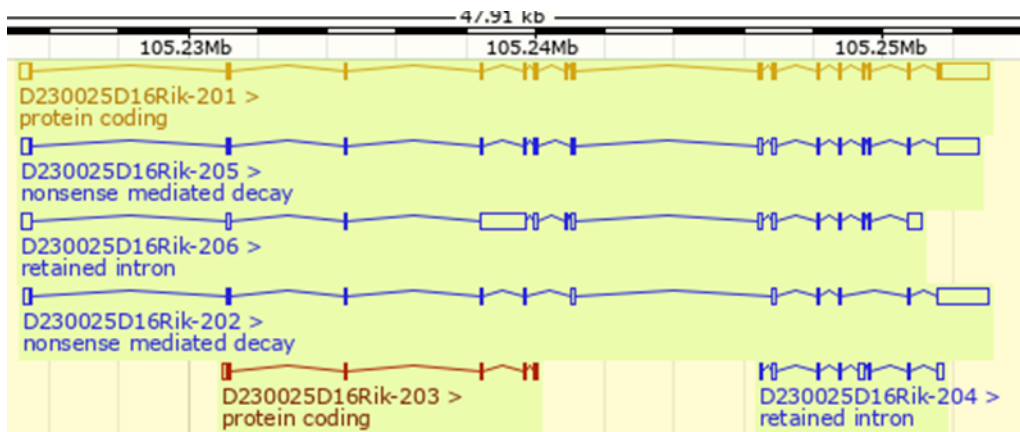


FIGURE 3



D230025D16 201 codes for 47.42 kDa protein
D230025D16 203 codes for 13.26 kDa protein

FIGURE 4

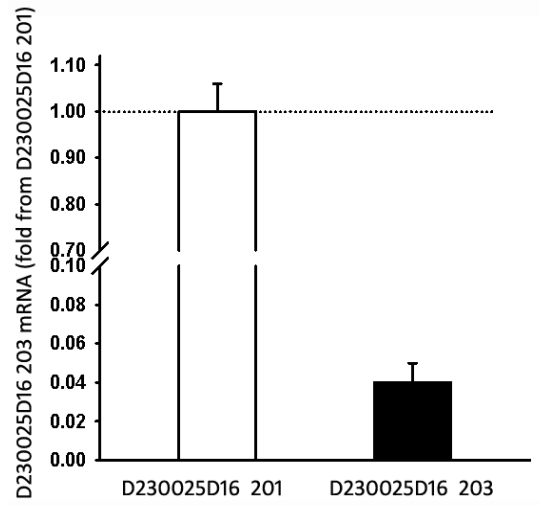


FIGURE 5

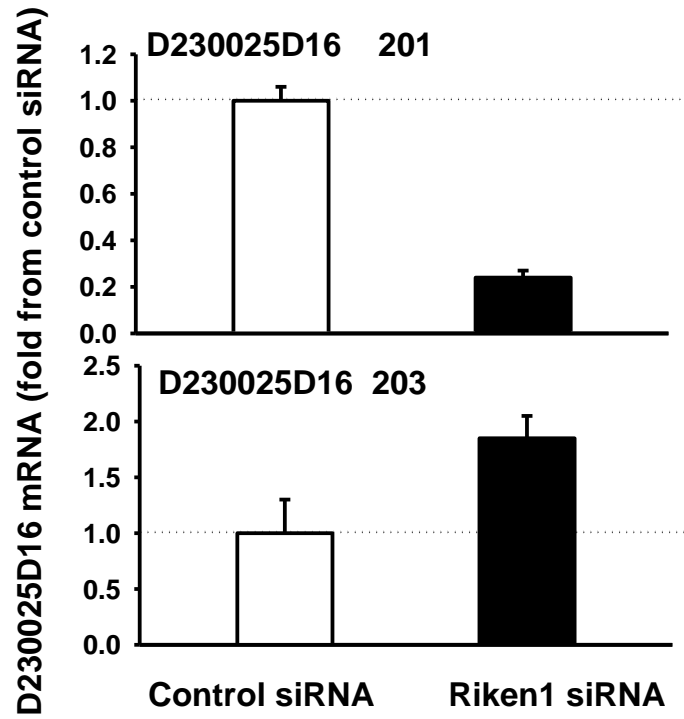


FIGURE 6

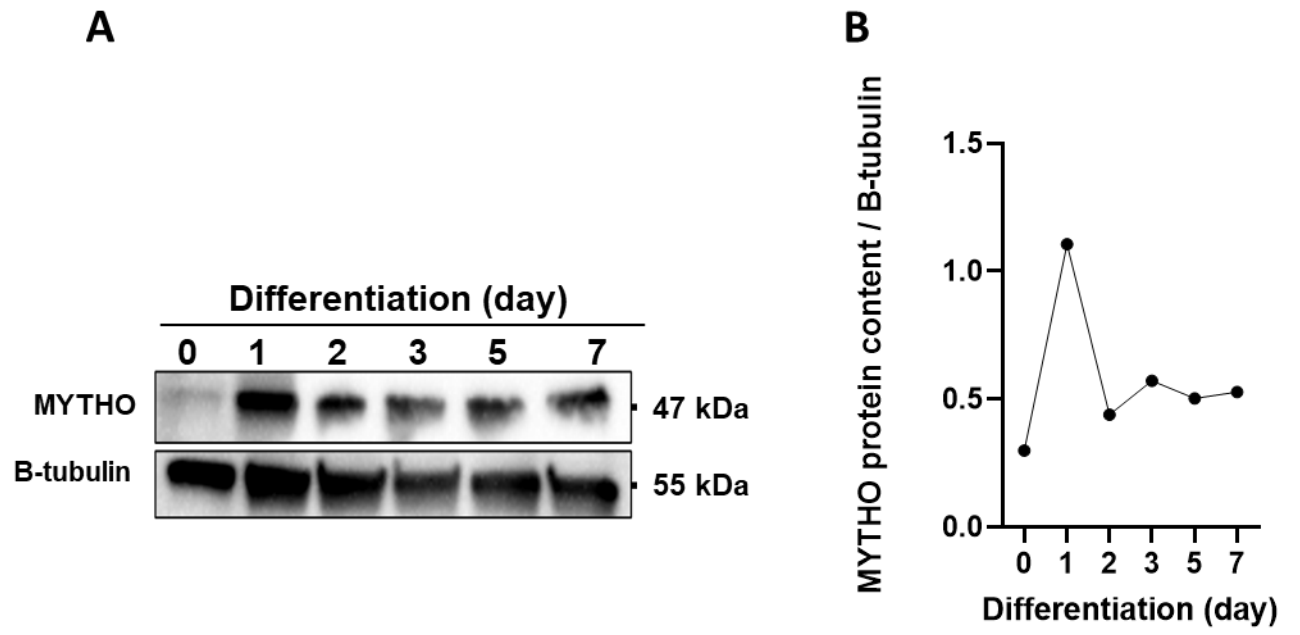


FIGURE 7

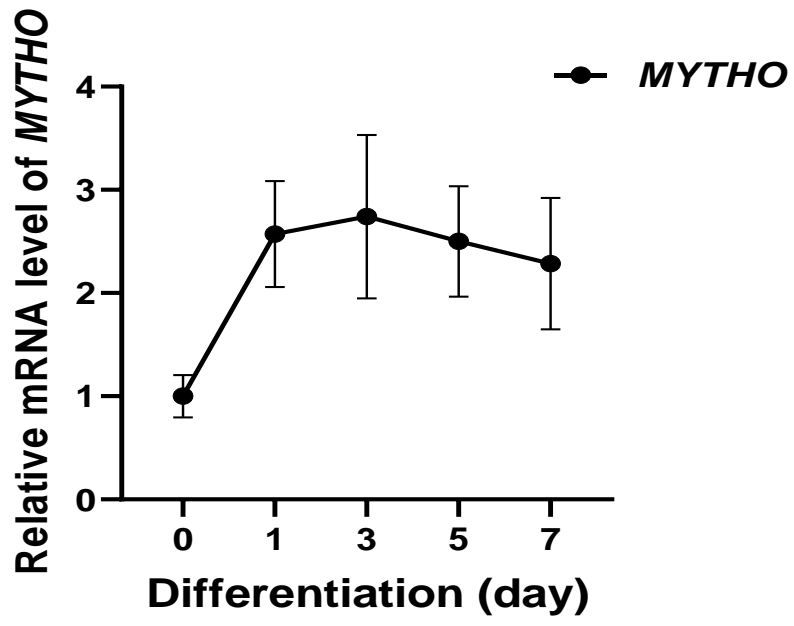


FIGURE 8

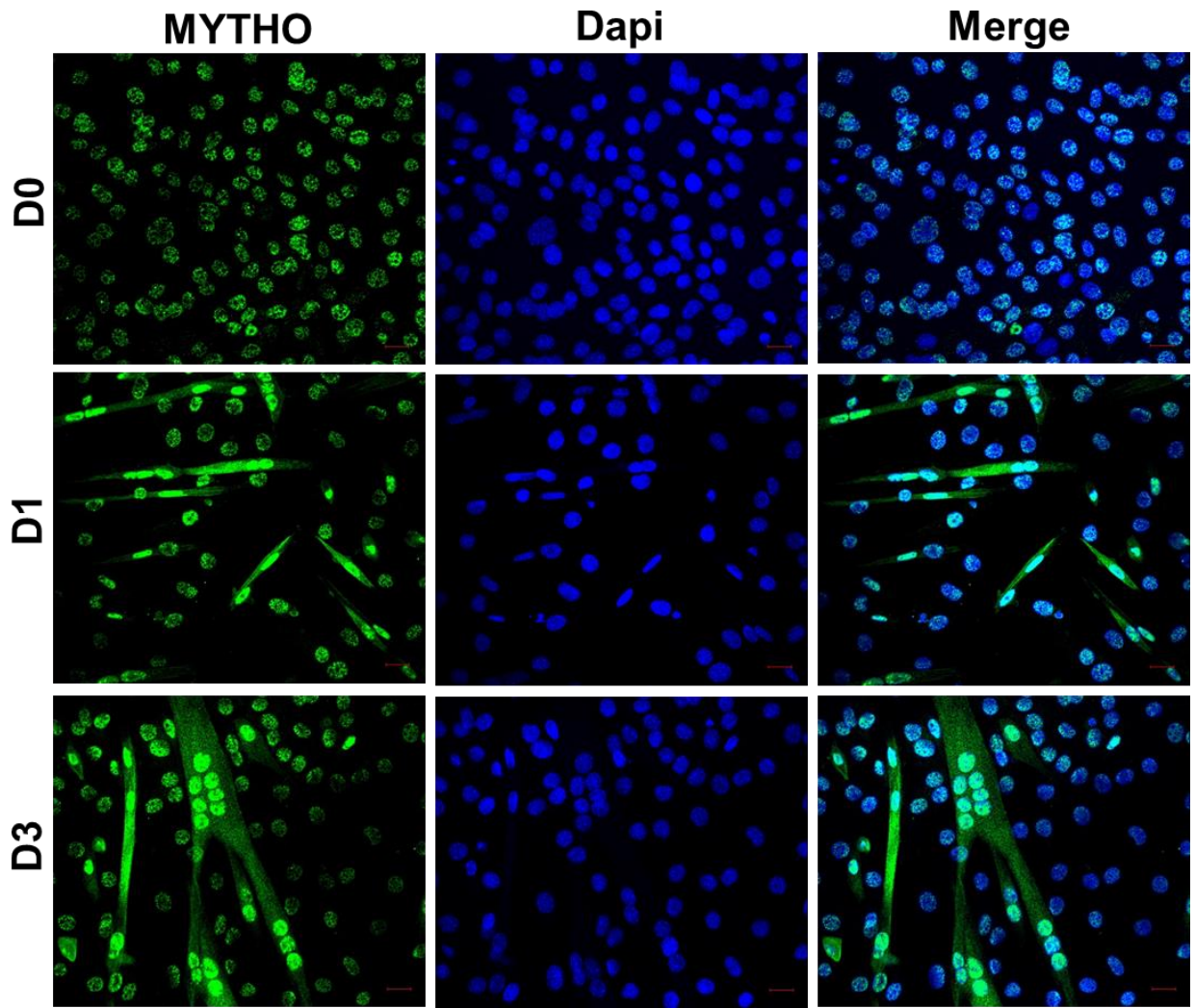


FIGURE 9

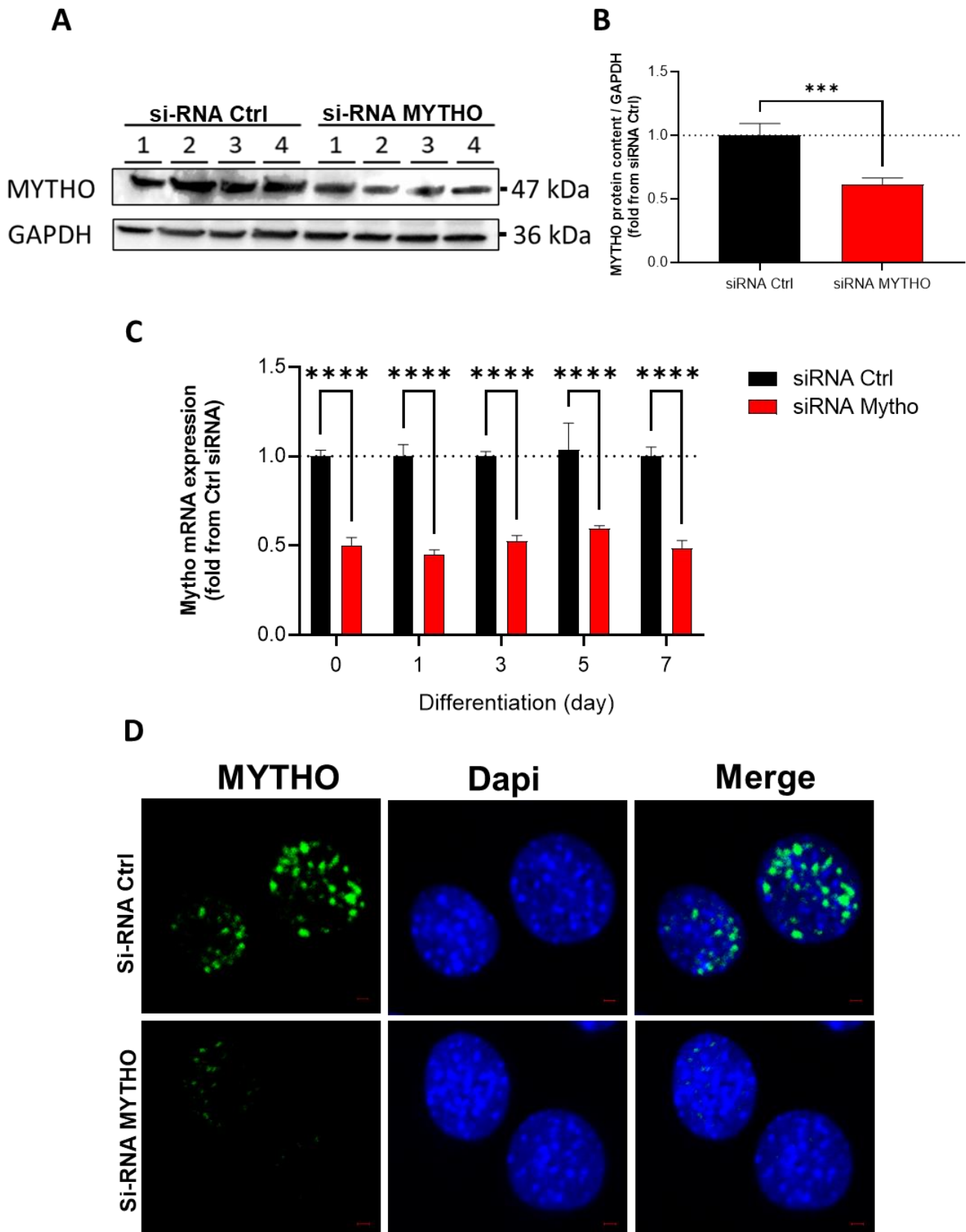


FIGURE 10

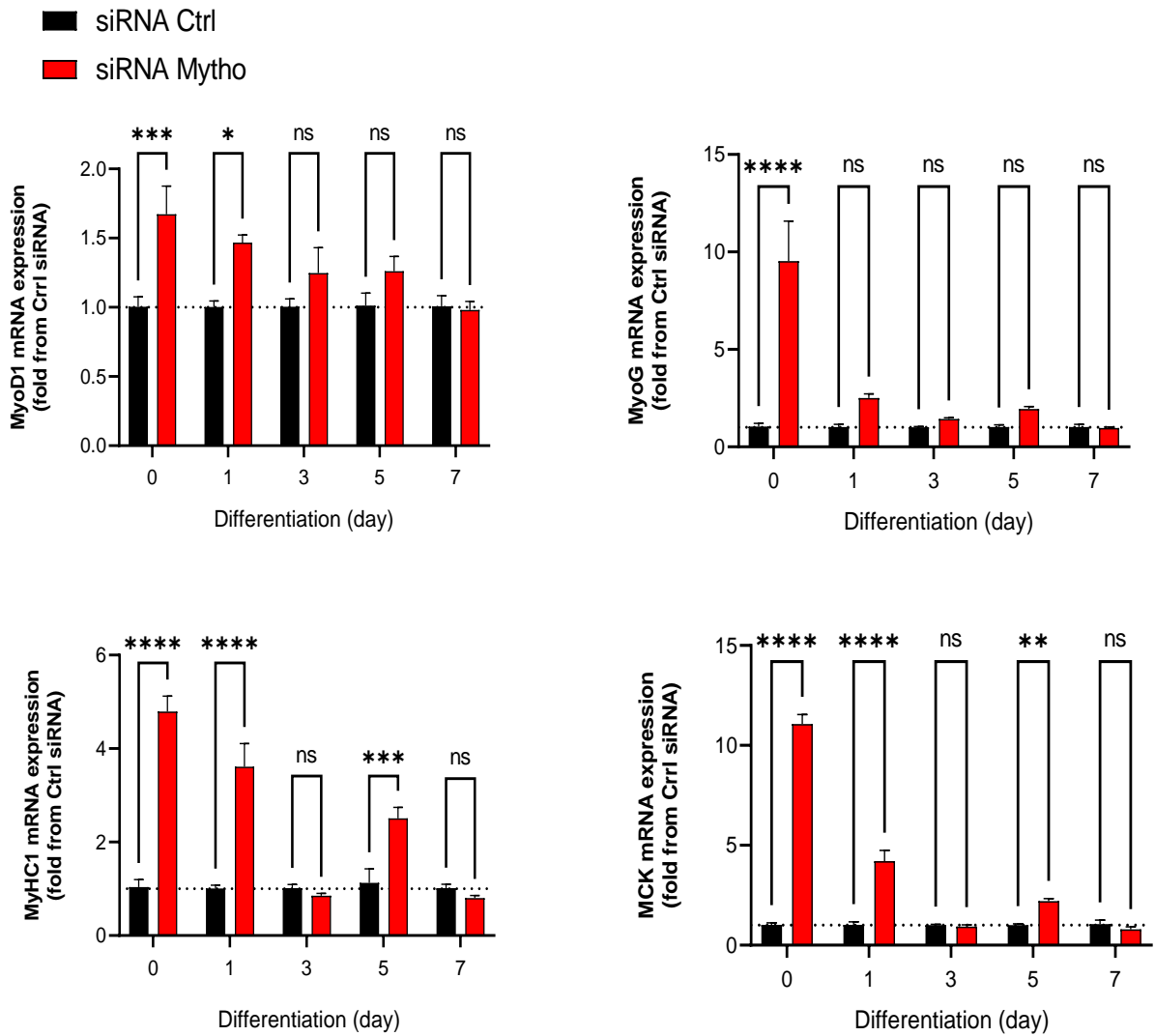
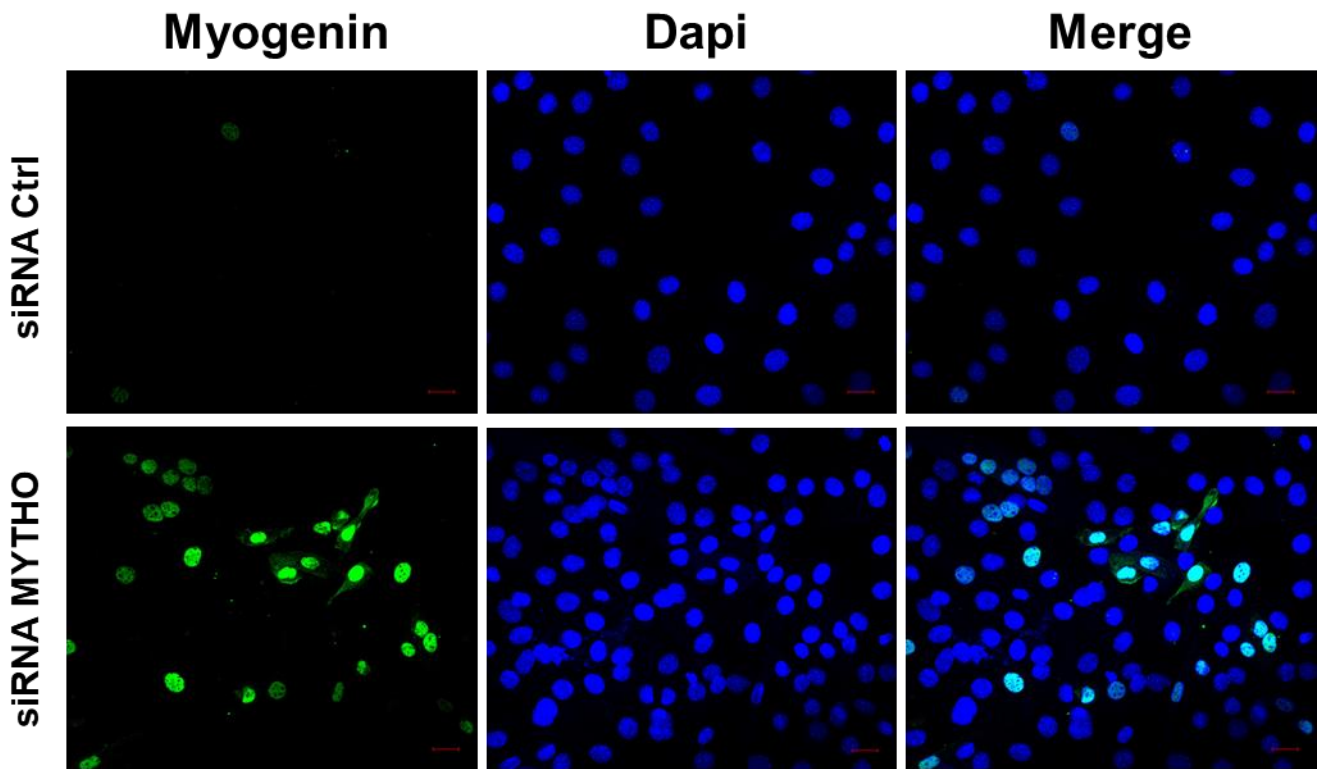


FIGURE 11

A



B

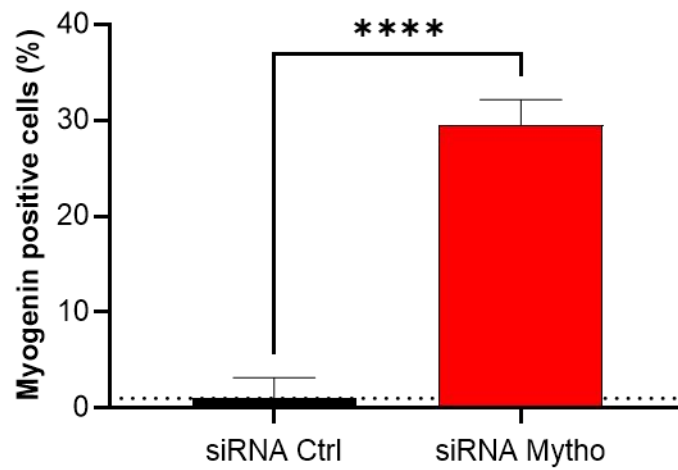


FIGURE 12

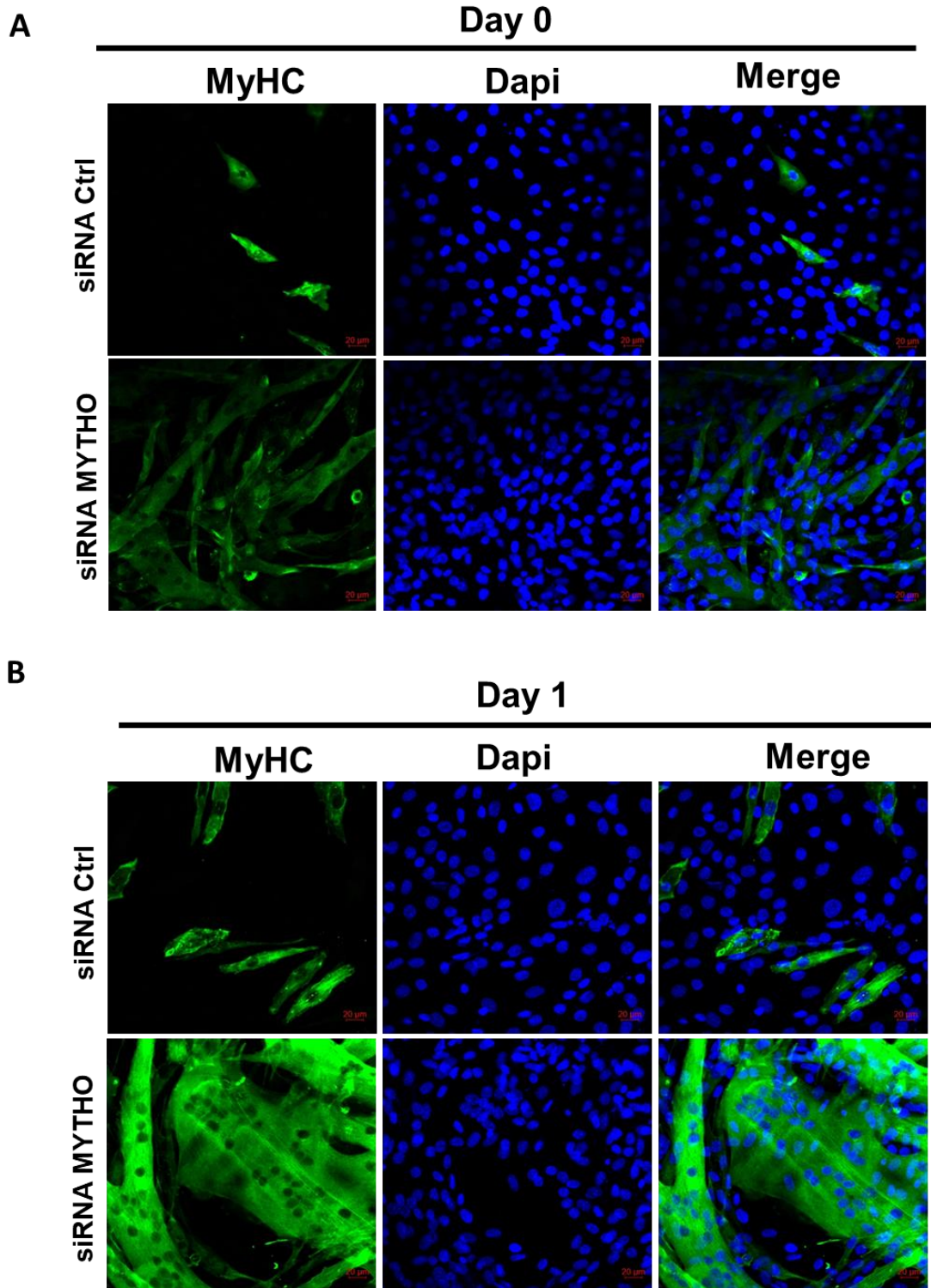


FIGURE 13

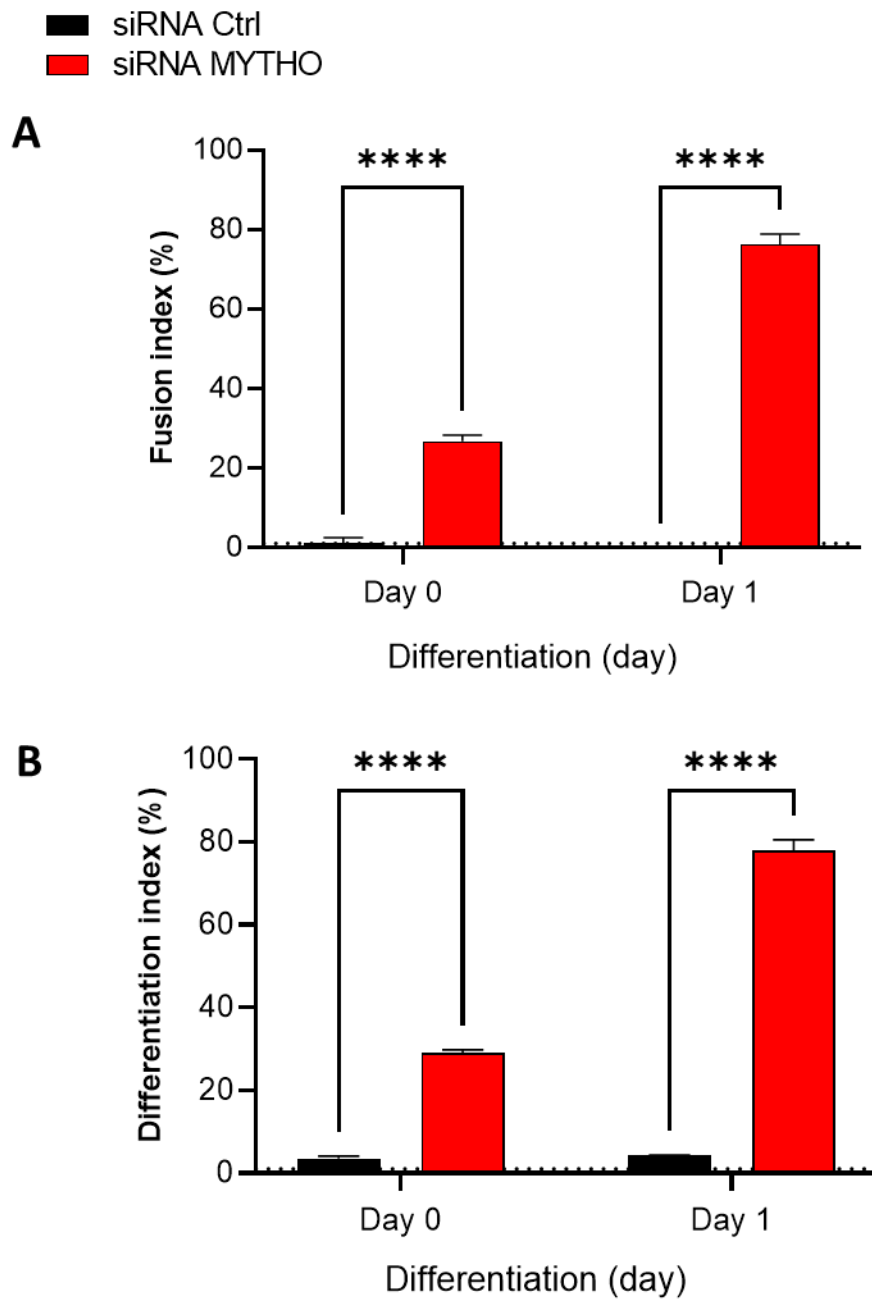


FIGURE 14

■ siRNA Ctrl
■ siRNA Mytho

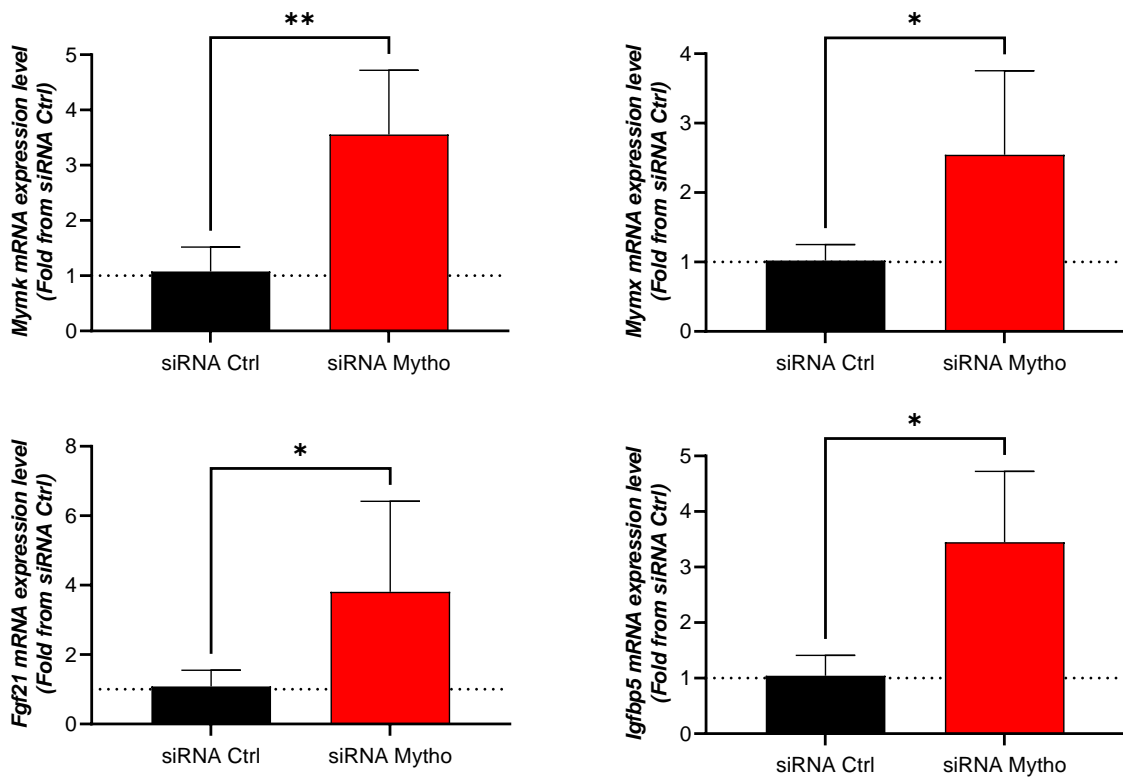


FIGURE 15

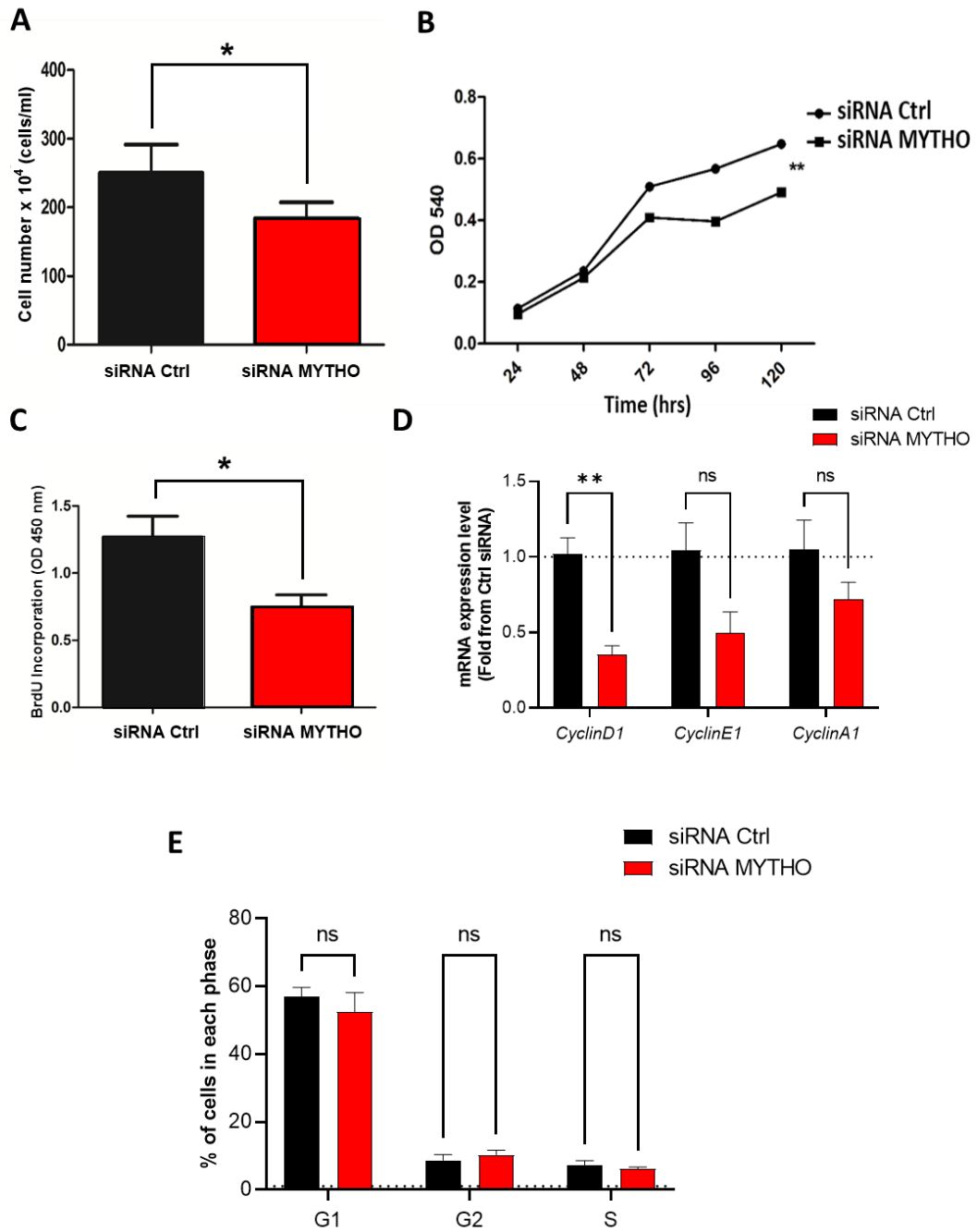


FIGURE 16

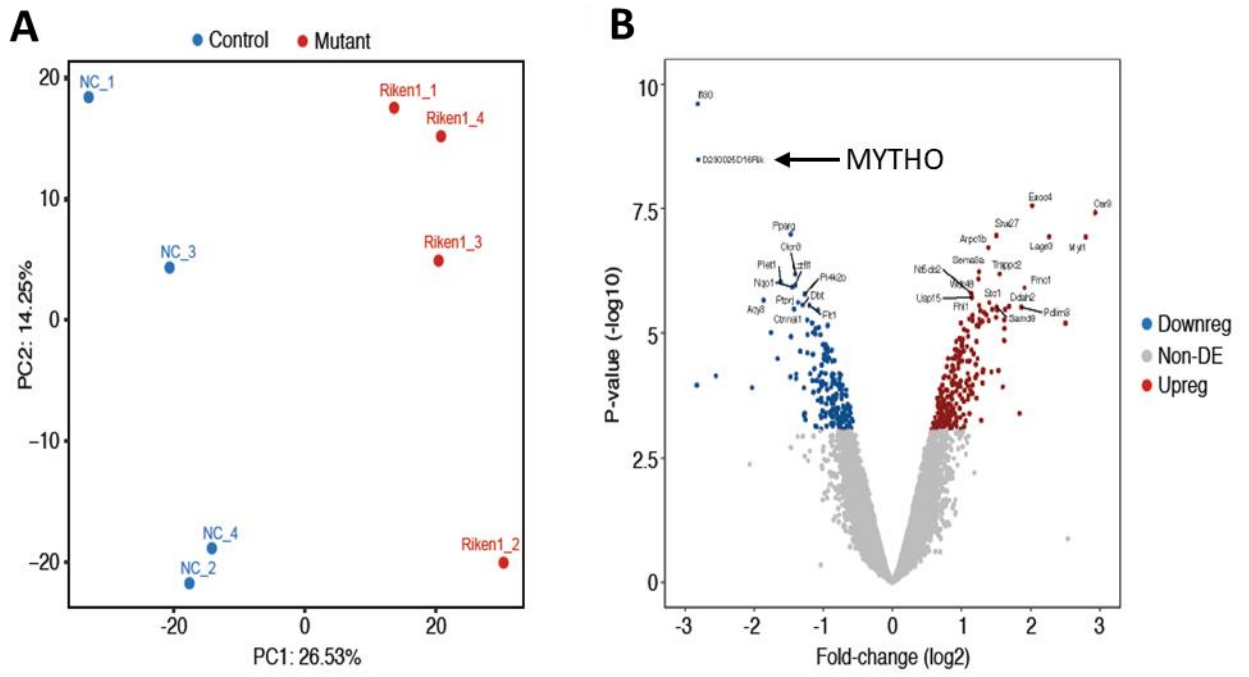


FIGURE 17

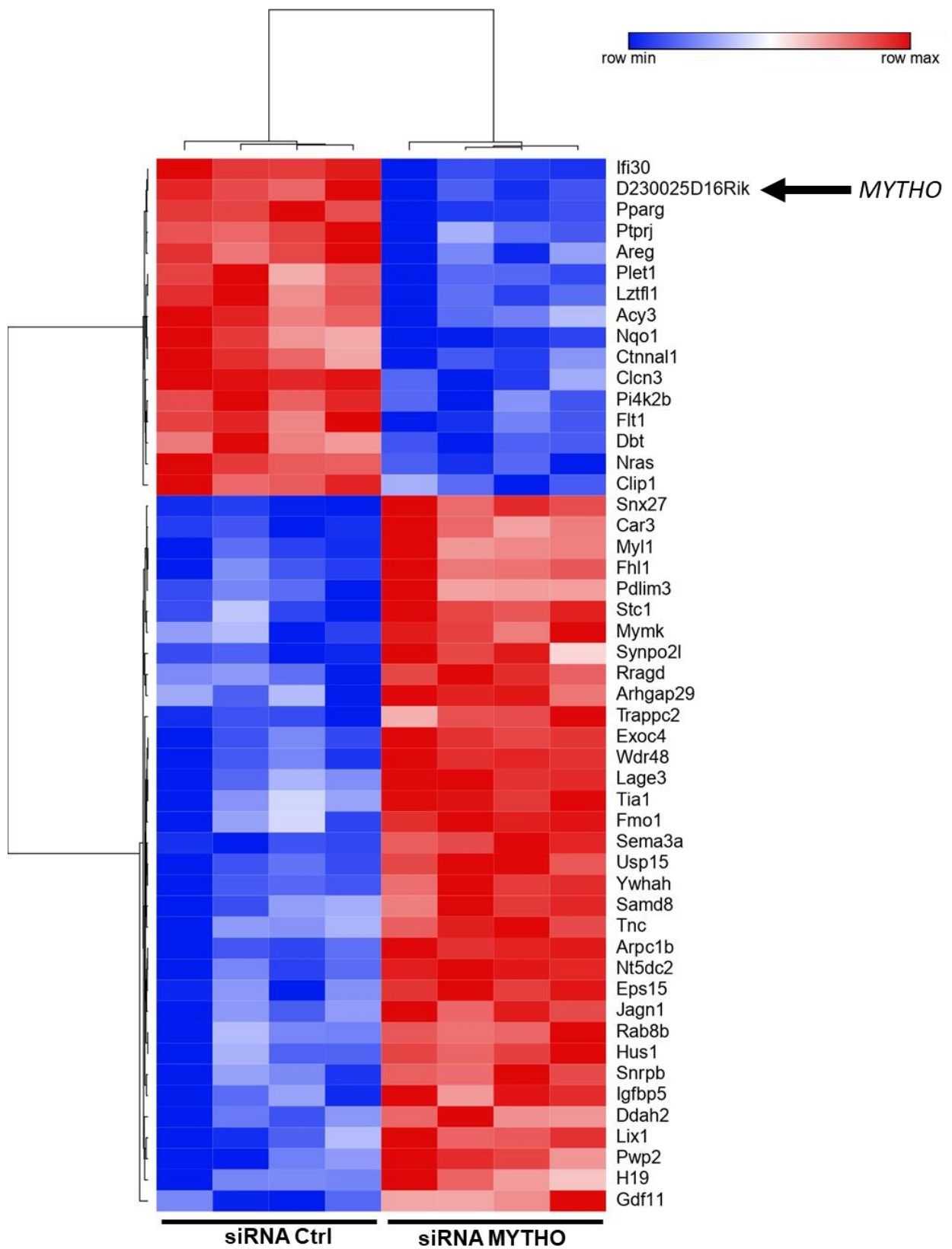


FIGURE 18

GO - Biological process

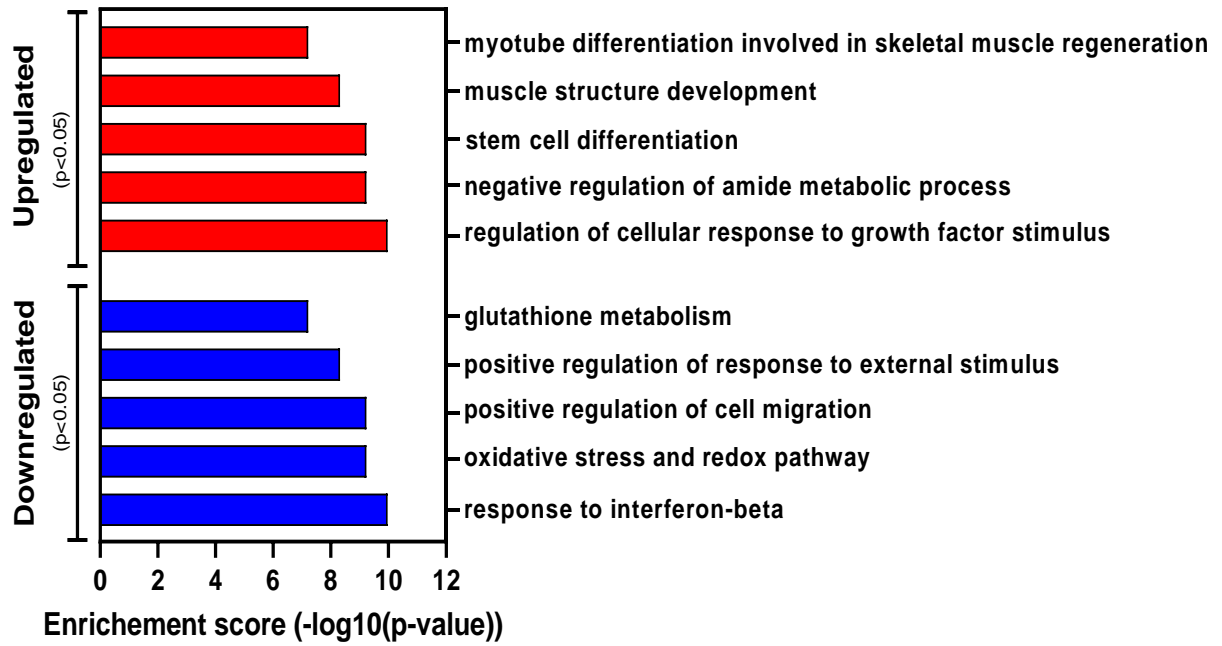


FIGURE 19

Muscle cell growth and development genes
($p < 0.05$)

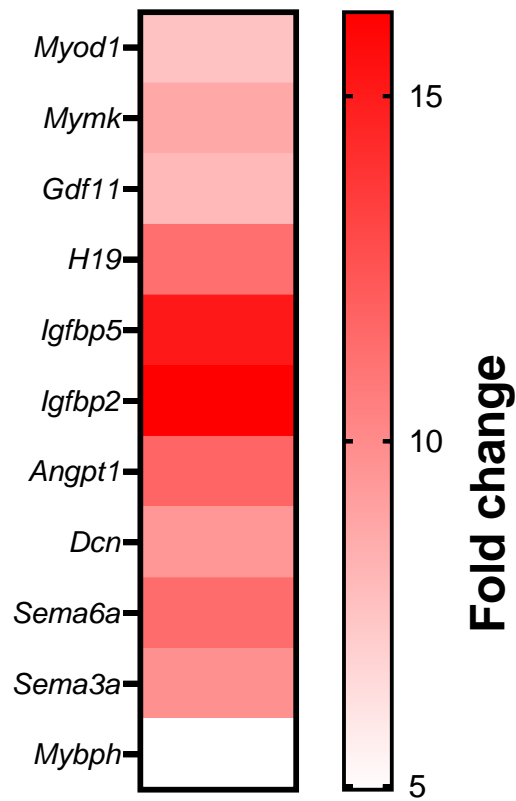


FIGURE 20

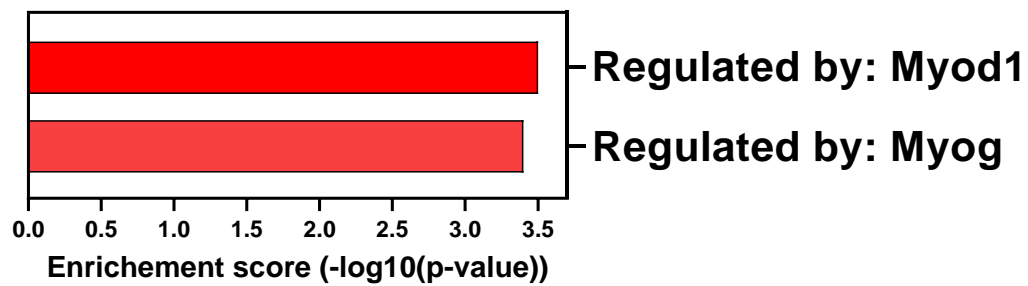


FIGURE 21

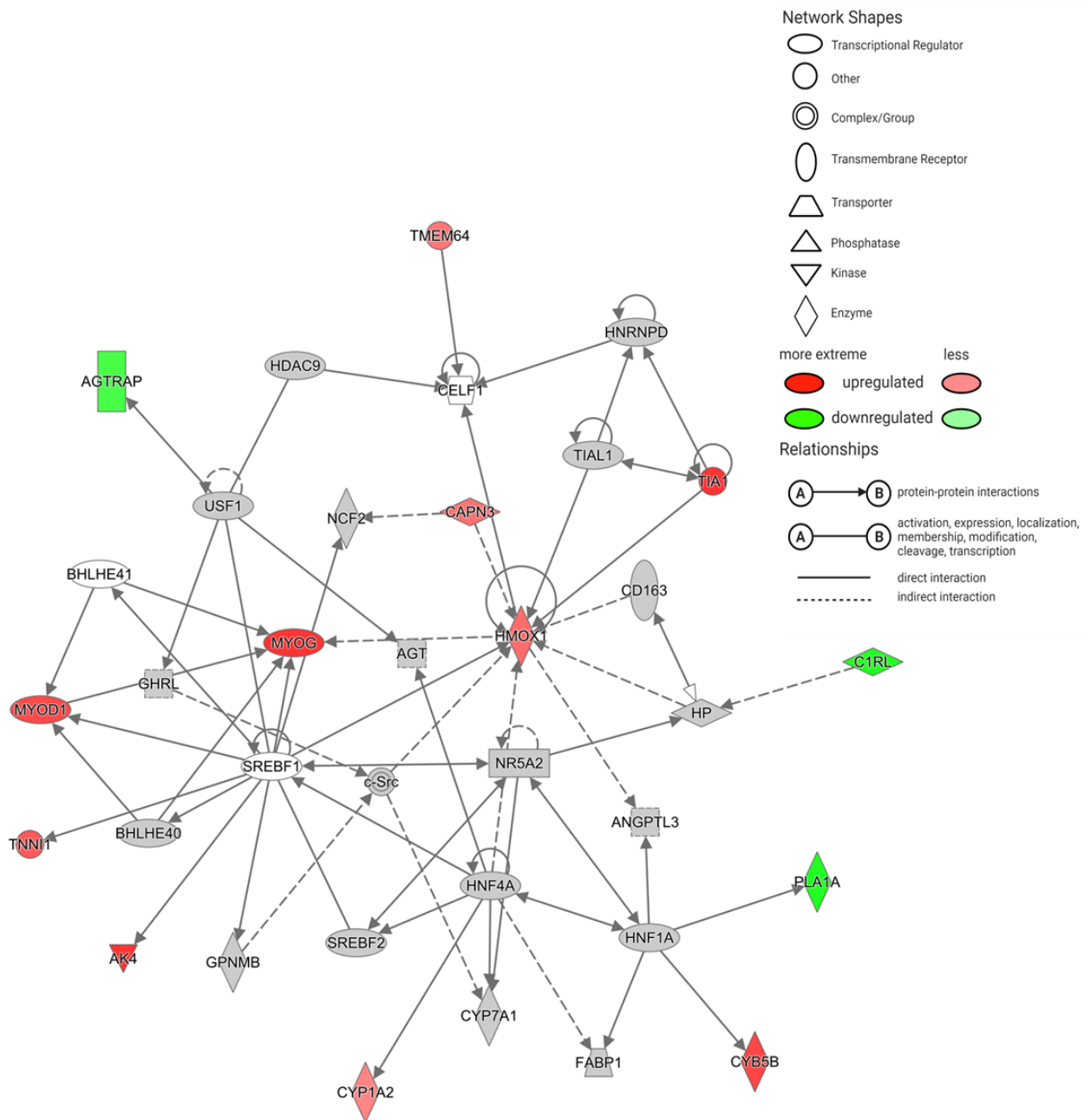
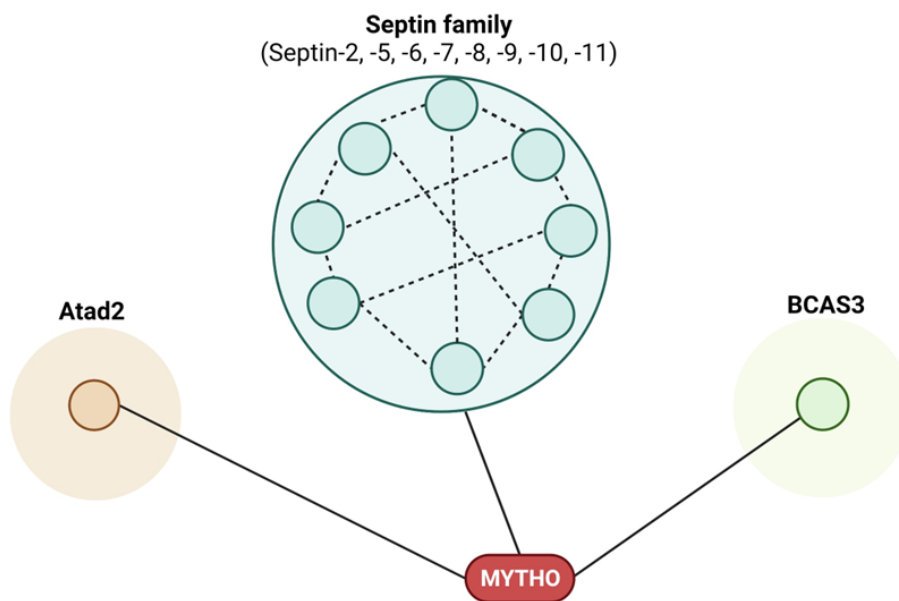


FIGURE 22

A

Protein name	MW (kDa)	Accession number	Day 0	12hr	Day 5	IgG
Septin7	51	O55131	184	152	291	
Septin2	42	P42208	126	123	244	
Septin9	66	Q80UG5	125	123	211	
Septin11	50	Q8C1B7	103	107	178	
Septin6	50	Q9R1T4	46	46	79	1
Septin8	50	Q8CHH9	61	62	116	
Septin10	52	Q8C650	26	25	39	
BCAS3	101	Q8CNN5	21	15	43	
Atad2	118	C8CDM1	31	26		
Septin5	43	C9Z2Q6	3	2	6	

B**FIGURE 23**

SECTION 8: FIGURE LEGENDS

Figure 1: Satellite cell activation, proliferation, differentiation, and fusion into new myofibers.

The figure was created with BioRender.com.

Figure 2: Myogenic lineage progression is characterized by differential expression patterns of myogenic regulatory factors and paired box proteins. The figure was created with BioRender.com.

Figure 3: A: The sequence alignment of MYTHO and conservation among species (*Homo sapiens*, *Rattus norvegicus*, *Mus musculus*). Performed using ClustalW and the image was produced using Easy Sequencing in Postscript (ESPrpt 3.0; <http://www.esprpt.ibcp.fr>); **B:** Bioinformatic predicted binding domains of MYTHO protein showing WD40 and LIR motifs. **C:** Predicted protein structure of MYTHO, retrieved from the I-TASSER database [143].

Figure 4: Visualization of six *Mytho* mRNA splicing variants (SV) using Ensembl (<https://ensembl.org/>), including mRNA D230025D16Rik-201 encoding for a 47-48 kDa protein, mRNA D230025D16Rik-203 encoding for a 13 kDa protein, and four mRNA splicing variants: mRNA D230025D16Rik-202, mRNA D230025D16Rik-205, mRNA D230025D16Rik-204 and mRNA D230025D16Rik-206.

Figure 5: qPCR analysis of *Mytho* isoform 201 and 203 expression levels in C2C12 myoblasts using selective PCR primers. Results in bar graphs are presented as means \pm SEM.

Figure 6: Selective knockdown of isoform 201 using si-RNA-mediated RNAiMAX transfection with oligos targeting D230025D16-201. Results in bar graphs are presented as means \pm SEM.

Figure 7: A: Representative immunoblot of MYTHO protein levels at day 0, 1, 2, 3, 5, and 7 of differentiation. B-tubulin was used as a loading control. **B:** Visualization of MYTHO protein level across myogenesis.

Figure 8: Means \pm SEM of mRNA levels of *Mytho* at day 0, 1, 3, 5, and 7 of differentiation.

Figure 9: Representative immunofluorescence staining of MYTHO on day 0, 1, and 3 of differentiation.

Figure 10: A&B: Representative immunoblot and mean \pm SEM of MYTHO protein level at day 0 in response to transfection with MYTHO siRNA and control siRNA. Glyceraldehyde-3-phosphate dehydrogenase (GAPDH) was used as a loading control. **C.** Means \pm SEM of mRNA levels of *Mytho* on day 0, 1, 3, 5, and 7, of differentiation in response to transfection with MYTHO siRNA and control siRNA. **D.** Representative immunofluorescence staining of MYTHO at 48 hours post transfection with MYTHO siRNA and control siRNA.

Figure 11: Means \pm SEM of mRNA levels of various myogenesis-related genes at 48 hours post transfection with MYTHO siRNA and control siRNA.

Figure 12: **A.** Representative immunofluorescence images of Myogenin at 48 hours post transfection with MYTHO siRNA and control siRNA. **B.** Means \pm SEM of the number of Myogenin positive myoblasts.

Figure 13: Representative immunofluorescence images of MyHC1 at day 0 and day 1 of differentiation in response to transfection with MYTHO siRNA and control siRNA.

Figure 14: **A.** Means \pm SEM of the fusion index calculation of day 0 and 1 myotubes in response to transfection with MYTHO siRNA and control siRNA. **B.** Means \pm SEM of the differentiation index calculation of day 0 and 1 myotubes in response to transfection with MYTHO siRNA and control siRNA.

Figure 15: Means \pm SEM of mRNA levels of various differentiation-promoting genes at 48 hours post transfection with MYTHO siRNA and control siRNA.

Figure 16: **A.** Means \pm SEM of the number of cells at 48 hours post transfection with MYTHO siRNA and control siRNA. **B.** MTT assay used to determine cellular proliferation of proliferating myoblasts in response to transfection with MYTHO siRNA and control siRNA across a time course of 24, 48, 72, 96, and 120 hours. **C.** BrdU incorporation assay used to determine cellular proliferation of proliferating myoblasts in response to transfection with MYTHO siRNA and control siRNA. **D.** Means \pm SEM of mRNA levels of various cell cycle genes at 48 hours post transfection with MYTHO siRNA and control siRNA. **E.** Quantification of cell cycle distribution at 48 hours post transfection with MYTHO siRNA and control siRNA analyzed by flow cytometry.

Figure 17: **A.** PCA from microarray of Mytho siRNA and control siRNA samples. **B.** Volcano plot of top differentially expressed genes.

Figure 18. Heatmap from microarray showing Mytho siRNA and control siRNA gene expression signatures. Colors indicate relative expression levels; red indicates high expression and blue indicates low expression.

Figure 19. Top five upregulated (red) and downregulated (blue) pathways upon MYTHO knockdown (MYTHO-KD) as identified through GO enrichment analysis.

Figure 20. Heatmap highlighting selected significantly upregulated genes known to be involved in muscle cell growth and development.

Figure 21. TRRUST analysis of 218 upregulated genes revealing transcription factors MyoD1 and Myogenin as the top candidates.

Figure 22. Differentially expressed genes involved in interacting with MyoD1 and Myogenin directly or indirectly in response to transfection with MYTHO siRNA are listed in the IPA network. The brightness of color is related to the fold change.

Figure 23. A. Identification of potential MYTHO-associated proteins in myoblasts, myoblasts deprived of growth factors for 12 hours, and day 5 myotubes. **B.** Visualization of interacting of MYTHO-associated proteins.